

**Griffith School of Engineering  
Griffith University**

**6002ENG – Industry Affiliates Program**

# **Lateral resistance of cold-formed steel portal frame using C-shaped section in residential framing industry**

**Huiyue Qiao, S5216336**

*13<sup>th</sup> June, Trimester 1, 2022*

**Company Name : Xstructe**

**Industry Supervisor Name: Dr Bin Wang**

**Academic Supervisor Name: Professor Hong Guan**

*A report submitted in partial fulfilment of the degree of Bachelor of Engineering (Honours)*

The copyright on this report is held by the author and/or the IAP Industry Partner. Permission has been granted to Griffith University to keep a reference copy of this report.



## **EXECUTIVE SUMMARY**

This report focuses on the investigation of the lateral load bearing capacity of a non-apex cold-formed steel (CFS) portal frame using the Finite Element Modelling(FEM) method and the static nonlinear analysis method. The designed portal frame has a span of 3.2 m and a height of 2.8 m and is composed of single C-shaped cross-sectional CFS members connected by bolts. The investigated CFS portal frame is designed to have no apex and can be installed into the residential building to work as the load-carrying structure. In this research, the applied lateral load is from wind only. The goal of this study is to reduce the use of expensive hot-rolled steel portal frames in residential building construction by introducing cold-formed ones, thus making building material delivery and on-site construction more cost-effective.

To explore whether the CFS portal frame is capable of working as the load-bearing structure in residential buildings, the research procedure was divided into three parts. Broad literature reviews were carried out first based on the characteristics of the CFS structures, material properties, damage modes, and analysis methods, and then more concentrated explorations on the past studies of CFS portal frames using FEM methods were carried out. Then the FEM method was chosen to simulate the strength behaviour of the CFS with high accuracy. A full-scale model was built using Quad4 elements in Strand7, with rigid link elements working as idealised connectors. Validation tests of the modelling accuracy and rigid link elements were also performed. After that, the static nonlinear analysis method considering geometrical and material nonlinearity was carried out for the structure, and different mesh sizes were applied to carry out a convergence study. Finally, the load-displacement relationship and the deformed shapes from the most accurate result were discussed in detail by considering the effects of real bolts.

The simulated results showed that the single C-section CFS portal frame can sustain the lateral load efficiently to a very large value if the whole structure is ideally connected. The perfectly composed structure itself is durable enough for residential use, which can bear an ultimate load of 1.2MPa eventually. In reality, however, structures are not always ideally composed, and this will be reflected in the tearing of CFS plates around the location of bolts if the bolts sustain excessive loads. Further research on the bolt efficiency and the load-bearing capacity from other directions is still needed to gain a full understanding of the strength behaviour of the single C-shaped cross-sectional CFS portal frame.

## **ACKNOWLEDGEMENTS**

I extend my deepest and sincerest gratitude to my academic supervisor, Professor Hong Guan, for her invaluable guidance through my research. It is a great honour and privilege to finish my undergraduate dissertation under her supervision. I would like to thank her for her patience in guiding me through the process of research and providing me with all the helpful suggestions. I am also thankful to her kindness for offering useful learning materials, which helped me understand my research better. I feel very grateful for her support for my IAP project.

I also gratefully acknowledge the support from my industry supervisor, Dr. Bin Wang. I appreciate his willingness to offer the IAP project topic to me and share his innovative ideas about the research. I appreciate that he took time out of his busy schedule to discuss my report with me and answered all my questions with great patience. I sincerely thank him for all his support and suggestions on my IAP project.

Finally, I am deeply indebted to my family, who offered the financial support for me to continue my studies abroad in Australia. Without their physical and emotional support, I could not finish my studies. I sincerely thank them for their dedication and anticipation.

---

**TABLE OF CONTENTS**

<b>EXECUTIVE SUMMARY .....</b>	<b>I</b>
<b>ACKNOWLEDGEMENTS .....</b>	<b>II</b>
<b>TABLE OF CONTENTS .....</b>	<b>III</b>
<b>1 INTRODUCTION .....</b>	<b>1</b>
<b>1.1 Project background .....</b>	<b>1</b>
<b>1.2 Research aim and objectives .....</b>	<b>3</b>
<b>1.3 Overview of research scope and methodology .....</b>	<b>4</b>
<b>1.4 Thesis structure .....</b>	<b>5</b>
<b>1.5 Research accomplishment .....</b>	<b>5</b>
<b>2 LITERATURE REVIEW .....</b>	<b>6</b>
<b>2.1 General .....</b>	<b>6</b>
<b>2.2 Cold-formed steel members .....</b>	<b>6</b>
2.2.1 Member properties - Stress-strain relationship of CFS sections .....	7
2.2.2 Twist and warping behavior of C-shaped cross sections .....	8
<b>2.3 Potential bulking modes in C-shaped CFS members .....</b>	<b>10</b>
2.3.1 Local buckling .....	11
2.3.2 Global buckling .....	11
2.3.3 Distortional buckling .....	12
2.3.4 Buckling analysis methods .....	12
2.3.5 Post-buckling inelastic reserve capacity for CFS .....	13
2.3.6 Buckling behavior of CFS members with C-shaped cross sections .....	13
<b>2.4 Cold-formed steel analysis .....</b>	<b>14</b>
2.4.1 First-order elastic analysis .....	15
2.4.2 Elastic buckling analysis .....	16
2.4.3 Second-order elastic analysis .....	17
2.4.4 Plastic analysis .....	18
2.4.5 Advanced Analysis .....	19
<b>2.5 Cold-formed steel portal frames .....</b>	<b>21</b>
<b>2.6 Summary of literature review and the research gap .....</b>	<b>27</b>
<b>3 METHODOLOGY AND PORTAL FRAME MODELLING .....</b>	<b>28</b>
<b>3.1 Overview .....</b>	<b>28</b>

<b>3.2 Theoretical base .....</b>	<b>29</b>
<b>3.3 Finite element modeling .....</b>	<b>30</b>
3.3.1 Modeling approaches .....	30
3.3.2 Validation of rigid link elements .....	36
3.3.3 Verification of the portal frame model accuracy .....	37
<b>3.4 Summary .....</b>	<b>39</b>
<b>4 NUMERICAL ANALYSIS RESULTS .....</b>	<b>39</b>
<b>4.1 Convergence study .....</b>	<b>39</b>
<b>4.2 Load-displacement relationship and portal frame deformation shape .....</b>	<b>41</b>
<b>4.3 Estimation of the true frame strengths considering bolt capacity .....</b>	<b>44</b>
<b>5 CONCLUSION .....</b>	<b>47</b>
<b>6 REFERENCES .....</b>	<b>50</b>
<b>7 APPENDIX .....</b>	<b>54</b>

# 1 INTRODUCTION

## 1.1 Project background

Cold-formed steel (CFS) structures are fabricated by rolling plate steel into different shapes at environmental temperatures, which could provide more resistance for the material consequently. The production history of CFS structures has lasted for more than a century (Hancock, 2003). In general, CFS section profiles of Cee, Zee, I, Tee shapes, angles, hat shapes, and tubular shapes, as shown in figure 1, are widely used when manufacturing structural frames. Meanwhile, compared with hot-rolled steel sections, CFS can be milled into more irregular shapes at lower costs. As a result of this, advantageous strength-to-weight ratios can be acquired. Also, it is possible to produce segments that can be nested reasonably to achieve intensive assembly, and this makes transportation easier and more efficient to some degree (Yu et al, 2020). Due to the cold forming procedure, CFS can be rolled into certain precise shapes to fulfill more specific requirements in both profiles and strength, and makes delivery easier.

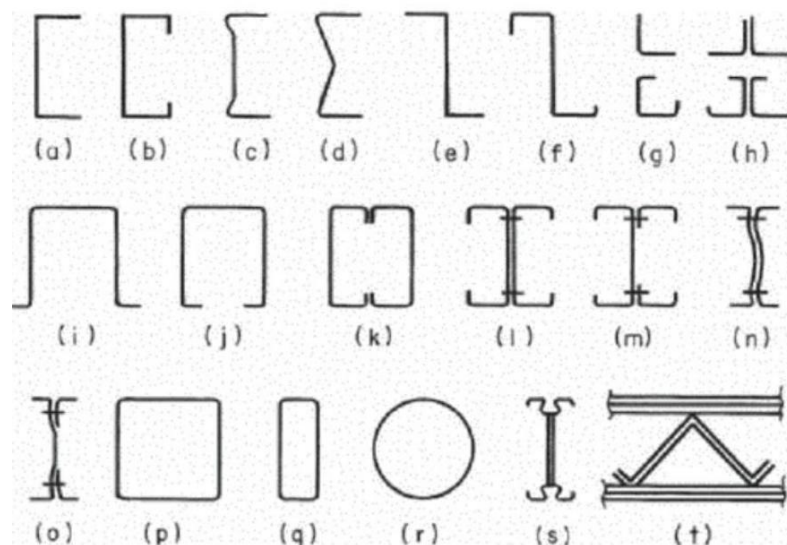


**Figure 1. General sections of CFS structural frames (Yu et al, 2020).**

Nowadays, in the construction industry, light-gauge steel frames manufactured by CFS profiles coated with zinc are applied extensively and now their usage is penetrating to housing construction, which would gradually replace the use of masons and under-supplied wood (Grubb et al 2001). Also, according to Phan et al. (2017), CFS has gained increasingly

popular usage in low-rise building constructions and the proportion of CFS buildings in all steel constructions would attain 70% in the recent few years.

In building constructions, light gauge structures usually play the main role in non-load bearing structures. And gradually, they are being applied for structural usage in more and more cases (Harini et al, 2020). Moreover, the advantageous flexibility of CFS in the cross-section optimization during the manufacturing process also helps improve the load-carrying capacity for CFS members (Ye et al., 2016), which makes the material more capable of working as a load-resisting material in structures. Among CFS structures of various profiles, C-shaped built-up cross-sectional portal frames normally have the ability to achieve the required lateral resistance in wall panels (Baran & Alica, 2012). Some experiments also concluded that CFS can work as an alternative for hot-rolled steel in the construction of industrial and residential portal frame buildings below a span of 15 m (Dundu, 2011). In the situation of the real-world construction, however, costly hot-rolled Parallel Flange Channel (PFC) portal frames are often used in light-gauge steel buildings to provide lateral resistance in most cases, which could also add labor and time inputs due to the need for on-site welding works

This project has an aim to accomplish a new mode of cost-effective residential construction by replacing the hot-rolled PFC portal frames, which are usually used in the structural system of a residential building, with CFS portal frames of open C-shaped profile. However, since the limitation of the lateral load capacity of light-gauge steel hinders its development in constructing civil buildings (Zhang et al, 2015) and it is widely believed that CFS is too thin to form the structural system, the finite element modeling (FEM) method is used to simulate and investigate the deflection of the structure and help to conduct the nonlinear static analysis on the portal frame for the estimation of the lateral resistant performance. Rigid link elements in Strand7 are used to compensate for the modeling simplification of bolt connections at eaves joints.

The span of the investigated CFS single C-section portal frame is designed to be 3.2 m with a height of 2.8 m to suit the dimension of the structural frame system in regular residential houses. To better fix the portal frame inside the residential building, the CFS portal frame has a similar shape to the hot-rolled PFC one, which has only one beam connecting two columns

on the opposite sides with no apex. The picture in Figure 2 shows the outlook of the common red-painted hot-rolled PFC portal frame applied in residential houses on the ground floor to sustain weight from the upper direction and the lateral loads. This project only explores the strength performances of the CFS portal frame when carrying lateral forces. The lateral loads used in this project are designed to be caused by wind, as the project would focus mainly on the residential construction in Australia, which is not an earthquake-prone region.

Dr. Bin Wang is the industry supervisor for this IAP course who provided the topic of the project. He is a Chartered Structural Engineer having 16+ years' post-graduate working experience in the engineering and construction industry in Australia and China.



**Figure 2. Frame and wall structures of a domestic building, by Huiyue Qiao.**

## **1.2 Research aim and objectives**

The cost of construction is mainly contained within financial costs and extra time in delivery and on-site construction. To reduce these costs, this project has a plan to explore if the single C-section CFS portal frames are able to work as the major load-bearing structures in residential construction and work as replacements for the hot-rolled PFC portal frames and even CFS braced walls in the light-gauge steel frames. The common residential construction combining CFS braced walls and PFC portal frames can be seen in Figure 2, where the

painting-coated PFC portal frames (red ones) have thicker profiles while the CFS structures in silver color look more light-weight and convenient.

The objectives of this project are divided into the following several parts. Firstly, a convergence study on the efficiency and accuracy of the results using different numbers of mesh elements will also be included, and the results will be presented visually. Secondly, the most accurate load-displacement relationship of a typical node with the largest horizontal displacement in the portal frame will be displayed as visualized pictures using Strand7, and the relationship between the expected wind load input and the critical loads regarding the yield strength and the ultimate capacity of the structure will be found. Thirdly, the global shape of the deformed portal frame which is proved to have the most accurate results from the convergence study will be exported as pictures and examined to find out the main causes behind large deflections and the final failure, and analysis on the effect of bolts will also be conducted on this model to provide an estimation of the structure behavior considering the installation of real bolts.

### **1.3 Overview of research scope and methodology**

This research focuses on the exploration of the lateral resistance of the CFS single C-section portal frames used especially for residential houses. Comprehensive literature reviews will be provided on the single C-sectional CFS member properties and past research about CFS portal frames using FEM and numerical analysis methods. In this case, the lateral force resistant response of the CFS portal frames will be investigated by modeling a physical portal frame in full-scale using Quad4 elements and rigid link elements as connectors in Strand7. Meanwhile, static linear analysis will be conducted on the rigid link elements to verify their function of working as an idealized substitution for bolt connections. Also, a coarse meshed frame model will be used to check the accuracy of the structure. Static nonlinear analysis will be then conducted using the solver in Strand7 taking account of both the geometrical shape and material non-linear nature of the members. Incremental loads will be applied to the portal frame for a gradually formed strength response. After that a convergence study will be carried out considering the contribution of different mesh sizes and the true structure capacity will be estimated taking into account the bolt strength.

#### **1.4 Thesis structure**

This research report starts with a research introduction in Chapter 1 and contains other 4 chapters on whole the research process.

In the following Chapter 2, a comprehensive knowledge base for the research subject and research method is provided. The CFS material properties regarding to its strength behavior are introduced and possible twist and buckling behavior for C-shaped sections are included. Also, the theory behind the software numerical analysis technique which is used in Chapter 3 to conduct the static nonlinear analysis on the finite element model is introduced.

Chapter 3 provides a valid methodology linking well to the project aim and objectives mentioned before. The research methods mainly contain building the research theoretical base with reviews on past studies, modeling the research subjective using finite elements, and validating the efficiency of the model and rigid link elements under Strand7 static linear solver operation. Comprehensive contents of the literature review are provided in Chapter 2 including the theoretical details of the static nonlinear analysis method, so more description of the finite element modeling process and verification is presented in Chapter 3.

In Chapter 4, the numerical analysis results from Strand7 static nonlinear solver using idealized links are provided in a visualized way using load-displacement curves. The convergence study is carried out to show how the mesh size influences the results. Effects of bolts are concluded using manual calculations to provide a relatively real strength analysis for the structure.

Chapter 5 makes a conclusion for this research project and the importance of the results is emphasized. Lessons learned from the research process as well as further perspective of the research are discussed.

#### **1.5 Research accomplishment**

It is proved in the simulation that the stability of the portal frame structure made by CFS elements with mono-symmetrical C-shaped cross-sections can be trusted concerning its lateral resistance in residential buildings if all the members are tightly connected. Possible tearing of CFS plates near bolts may occur, however, due to the limited strength of bolts in

reality. This project also compensates for the limited research on the strength behaviour of thin-walled steel portal frames with no apex and single C-shaped cross-section members.

## **2 LITERATURE REVIEW**

### **2.1 General**

The literature review covers the contents of the material strength properties of CFS members and the twist behaviour of the single-C shaped cross-section under eccentric loading. Member warping happens attributable to the twisted cross-section and different member deformations are also classified into types of buckling modes, which are described briefly in this article together with the introduction of the post-buckling behaviour for lipped C-sections. Possible buckling behavior, especially concurring in the single symmetrical C-shaped sections, is also discussed. Concerning the large deformation of the loaded thin-walled steel structures, the nonlinear analysis method concerning geometrical and material nonlinearity and the initial geometry imperfections is recommended for use in this research, and all the analysis methods that helped to develop the final Advanced Analysis method are introduced in this part with discussions of their benefits and drawbacks. After presenting knowledge of the CFS member properties and analysis strategies, several past studies on CFS portal frames using the FEM method are provided to introduce a research development of recent years. The agreements and disagreements between the past research and the present research are evaluated at the end of the literature review to demonstrate the research gap.

### **2.2 Cold-formed steel members**

Steel members fabricated through the cold bending technology have more special characteristics, combining both advantages and disadvantages. Ductile CFS can be rolled into specific shapes to satisfy various construction objectives. At the same time, CFS members can be easily transported by stacking them wisely according to the cross-section shapes and can be assembled on site with relatively low costs. Despite the shaping advantages of the CFS members, certain geometries of the cross section may cause the member to twist under the eccentric loading and induce warping along the member. Moreover, the thin-walled character of CFS makes it more susceptible to large deformations as a result of the low stiffness.

In this part of the review, the stress-strain curve of CFS members is introduced to highlight the strength behaviour under progressive loading. Also, the twist and warping behaviour of the monosymmetric thin-walled member with the opening section caused by eccentric loads is analyzed, which also leads to the introduction of buckling modes and the post-buckling behaviour of CFS sections.

### 2.2.1 Member properties - Stress-strain relationship of CFS sections

The strength behaviour of CFS differs from that of hot-rolled steels. The stress-strain curve for the hot-rolled steel section tends to change sharply when the material yields and a yielding plateau is formed directly after that. The steel's yield stress is determined according to the level of the yielding plateau. However, contrary to the properties of hot-rolled steel, CFS usually has a progressively formed yielding plateau due to its cold-formed manufacturing process at the ambient temperature (Dabaon et al., 2015), which can be seen in Figure 3 with some fundamental material parameters involved. For CFS, the stress-strain relationship can be predicted using the two-stage Ramberg-Osgood model, which is introduced later in this article.

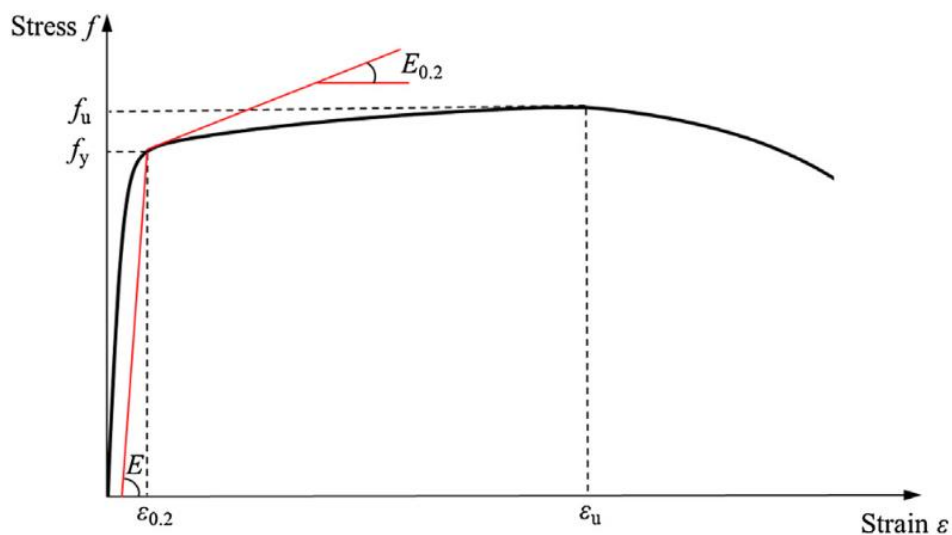


**Figure 3. Representative stress-strain curve for CFS (Dabaon et al., 2015).**

The original Ramberg-Osgood model (Ramberg & Osgood, 1943), which was further improved to be applicable to CFS by inserting its material parameters shown in Equation 1 below (Gardner & Yun, 2018), helps to estimate the stress-strain response for CFS using parameters when coupon tests are not available.

$$\varepsilon = \frac{f}{E} + 0.002 \left( \frac{f}{f_y} \right)^n \quad (1)$$

In Equation 1,  $\varepsilon$  represents the strain,  $f$  represents the stress,  $E$  is the Young's modulus,  $f_y$  represents the material yield strength which can be taken as the 0.2% proof stress, and  $n$  is the strain hardening exponent. The strain hardening exponent  $n$  shapes the round part of the stress-strain curve in the elastic-plastic region, which is determined by the equation below, where  $\sigma_{0.01}$  is 0.01% proof stress.

$$n = \frac{\ln(20)}{\ln(f_y/\sigma_{0.01})} \quad (2)$$

CFS tends to have a smoother stress-strain curve, ending with a higher ultimate strength. But less ductility is shown on certain parts of a section. Various material properties are shown at different cross section elements due to the diverse level of plastic deformation forming work. In particular, the corners of the cross section of CFS members may need greater plastic deformation, which contains more bending strength, to satisfy their narrow angular radius, and this can increase the strength but reduce the ductility of these parts accordingly (Gardner & Yun, 2018). A reasonable conclusion that can be made for the member element strength grading is that the corner areas of the CFS cross section are tougher than the elements around them, like flanges and webs, which also indicates that the corner radius is hardly changed during modes of buckling, and deformations of plate elements take a large part of the buckling shapes.

### 2.2.2 Twist and warping behavior of C-shaped cross sections

The C-shaped CFS sections only have a single symmetric axis in the cross sections, and the centroid centre and the shear centre do not meet together. Torsion occurs in this case as long as the transverse forces are not loaded directly pointed to the shear center, which could lead to further warping along the member (Gotluru et al., 2000). Together with the torsional moment around the shear center, which can be produced by timing the applied force ( $p$ ) and the distance between the force location and the shear centre ( $e$ ), a bending component is assumed to be an individual part of the twist behavior, which can be seen in Figure 4 (Rinchen, 2018; Hancock et al., 2001). Furthermore, if the torqued member has no constant restraints against torsion or lateral displacement, this member may fail under torsion together with warping (Gotluru et al., 2000).

The C-shaped CFS sections only have a single symmetric axis in the cross sections, and the centroid centre and the shear centre do not meet together. Torsion occurs in this case as long as the transverse forces are not loaded directly pointed to the shear center, which could lead to further warping along the member (Gotluru et al., 2000). Together with the torsional moment around the shear center, which can be produced by timing the applied force ( $p$ ) and the distance between the force location and the shear centre ( $e$ ), a bending component is assumed to be an individual part of the twist behavior, which can be seen in Figure 4 (Rinchen, 2018; Hancock et al., 2001). Furthermore, if the torqued member has no constant restraints against torsion or lateral displacement, this member may fail under torsion together with warping (Gotluru et al., 2000).

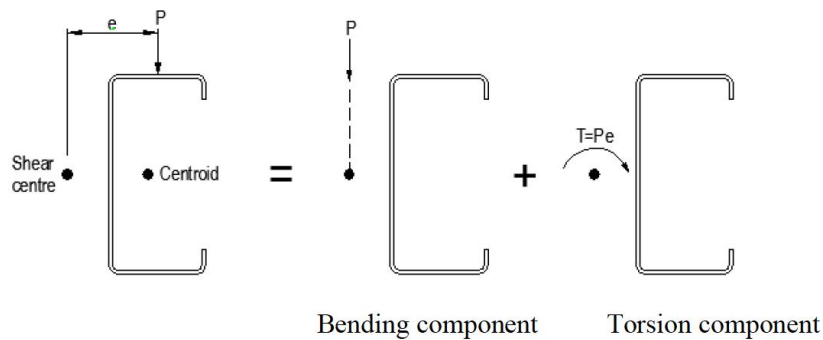


**Figure 4. Components of the eccentric force on single C-shaped section (Rinchen, 2018; Hancock et al., 2001).**

Figure 5 indicates a possible torsion shape of the C-shaped section, where the member is restrained to forbid translation along a specific direction and allow free rotations (Chu et al., 2004). This C-shaped section has a very similar restraint way and load condition to the laterally wind-loaded portal frame column explored in this research.

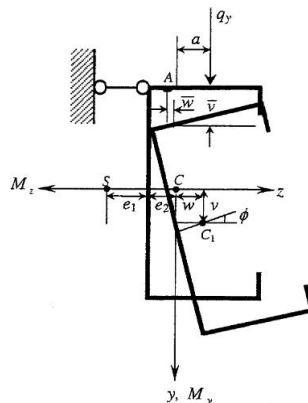


**Figure 5. Twisted C-shaped cross section with lateral translation restraints (Chu et al., 2004).**

The relationship between various kinds of moments and generalized strains is shown in the matrix equation below with reference to the picture above (Chu et al., 2004):

$$\begin{bmatrix} M_y \\ M_z \\ M_w \\ M_T \end{bmatrix} = \begin{bmatrix} EI_y & 0 & 0 & 0 \\ 0 & EI_z & EI_{wz} & 0 \\ 0 & EI_{wz} & EI_w & 0 \\ 0 & 0 & 0 & GJ \end{bmatrix} \begin{bmatrix} -\frac{d^2w}{dx^2} \\ -\frac{d^2v}{dx^2} \\ \frac{d^2\phi}{dx^2} \\ \frac{d\phi}{dx} \end{bmatrix} \quad (3)$$

This equation is developed with the centroid center working as the origin of the coordinate system, where  $M_y$  and  $M_z$  (bending moments around y and z axes respectively,)  $M_w$  (warping moment) and  $M_T$  (twisting moment) can be calculated by substituting the second moment parameters, displacement parameters and rotation parameters along each corresponding axis into the equation.

### 2.3 Potential bulking modes in C-shaped CFS members

When the thin-walled components (web and flanges) of a CFS member are subjected to compressive stress due to the external bending moments and axial forces, those parts of the member have a tendency to show in-plane deformation behaviour as well as out-of-plane responses if the element has low bending rigidity. The shape changes from each part of the member eventually form the deformation shape in the cross section, and this phenomenon can be classified as one of several buckling modes (Chen et al., 2007).

When compressive normal stresses appear in the whole or part of the cross-section, thin-walled steel members have a high potential to collapse due to structural instabilities. Overall, three major buckling modes can be identified from the deformation shapes of the cross-section, which are local buckling, distributional buckling, and global bulking, and every one of them may lead to the deformation of a structure and its ultimate failure (ÁDÁNY & SCHAFER, 2004). Figure 6 shows some examples of the deformation shapes of buckled C-shaped steel purlins under major axial bending.

In this part, different principal bulking modes that appear in the cold-formed members will be introduced and discussed separately. Also, methods applied for analysing the buckling modes would be described in broad terms. Then an analysis of the possible buckling performance specifically in the C-shaped build-up sections would be provided.

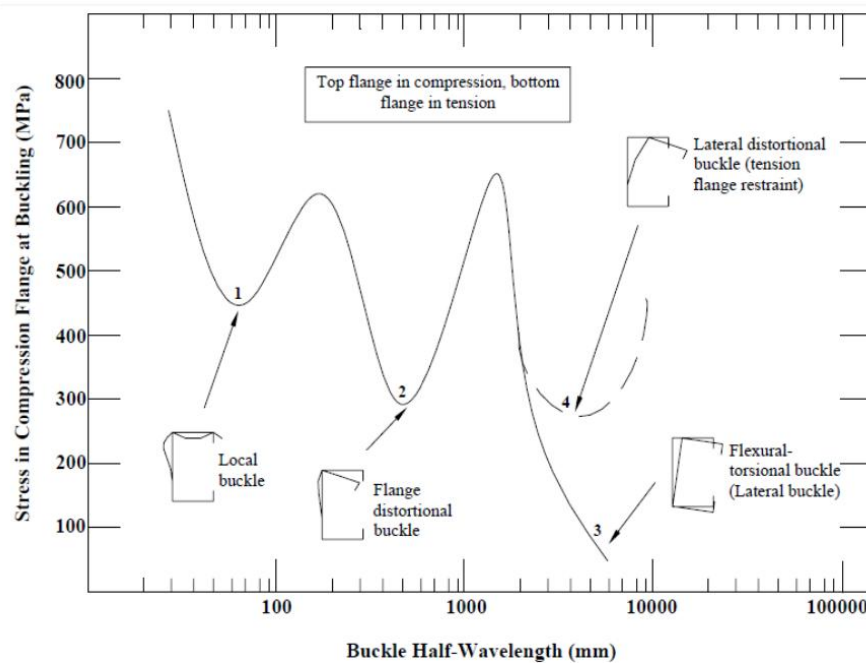


**Figure 6. Buckling modes of C-shaped steel beams under axial loads (Mohite & Karoo, 2015).**

### 2.3.1 Local buckling

Local buckling usually comes from plate bending moments, which develops out-of-plate deformations in the elements composing the cross section, with the fold lines at the junction of the adjoining element plates showing no translation (Naderian & Ronagh, 2015). This kind of buckling may not lead to instantaneous failure of a member, but it can cause fundamental stiffness reduction in the material and make it less capable under future compression loads and thus suffer early failure (Tan, 2001). The performance of local buckling can be seen in point 1 in Figure 6, and as is shown in the curve, the buckle half-wavelength of local buckling is the shortest compared with other buckling modes when the member is under compression. The buckle half-wavelength indicates the length of the buckling shape shown along the member (Chen et al., 2007), so from it the proportion of local buckling deformation that happens in a member can be easily deduced for long CFS beams.

### 2.3.2 Global buckling

In global buckling, no change is seen in the cross-section shape of a member while it deforms. The reason behind the constant cross-sectional shape is that the member deforms or twists laterally, following the classical beam theory. Some common global buckling types involve flexural, torsional, and flexural-torsional buckles for columns and lateral-torsional buckles for

beams (Naderian & Ronagh, 2015). An example of a flexural-torsional buckle shape can be seen at point 3 in Figure 6. The half-wavelength of global buckling is determined by the length of the unbraced member (Chen et al., 2007).

The particular mode of the global buckling appearing on part of the member is classified by its real bending or rotation manner and whether or not the external load is applied axially. Since the section deforms rigidly during global buckling, the failure may be little related to the yielding of the material, but more related to the elastic instability caused by changes in stiffness and geometry (Hancock et al., 2001).

### 2.3.3 Distortional buckling

Distortional buckling usually has a visual shape that combines local buckling and global buckling together, where some part of the section, like the flange, develops rigidity deformation around an intersection line but the other part, like the web, bends out-of-plate in a local buckling way (Chen et al., 2007). One of the typical distortional buckling shapes is indicated in point 2 in Figure 6, which also shows that all the corner nodes of the cross section are fixed.

### 2.3.4 Buckling analysis methods

Some numerical analysis methods have been developed in order to identify the different buckling modes shown on a loaded structure. One of the most popular methods is the Finite Element Method (FEM), which assesses the instability of the member using the fine mesh consistent of shell elements. This method involves iterations of increments of displacements or loads and takes account of residual forces (Camotim et al., 2005). However, the numerous elements in the FEM could make the calculation time-consuming as well as result in large numbers of buckling modes. In the meantime, FEM itself is unable to identify and classify the various buckling modes, so it's the users who distinguish the buckling modes manually with much effort.

The Finite Strip Method (FSM) software package can probably make up for the disadvantages of FEM by automatically giving out the function relationship between the derived critical loads and the buckling length. As a result, several lowest peak points in the function curve indicate different buckling loads, as shown in Figure 6.

Another new method named Generalized Beam Theory (GBT) can categorise the buckling modes and deduce the buckling stresses directly for thin-walled structures. But this method has low availability and fewer constrained assumptions, which reduces the applicability and accuracy of the method consequently (ÁDÁNY & SCHAFER, 2004).

This research focuses more on the global buckling shape of the structure and requires precision in the analysis results. So, the Finite Element Method was chosen for this research to make the model more detailed. The possible buckling mode that appears in the model is to be determined from the frame global deformation shape.

### 2.3.5 Post-buckling inelastic reserve capacity for CFS

In each CFS section element, the plate thickness is rather thin compared with the element width. As a result of the slender features of the thin-walled steel members, local buckling tends to appear quite earlier than the yielding of the steelwork sections, which, however, would not necessarily lead to the ultimate failure of the members. This kind of post-buckling performance is specifically effective for cold formed steel members having lips at the flange edges (Hancock et al., 2001). The build-up section of the cold steel members investigated in this research is C-shaped with two 28mm long lips orthogonally intersected with the upper and lower flanges respectively, so the discussion of the post-buckling strength is also included in this research.

As was mentioned before, the thin-walled steel sections would not reach their ultimate load capacity immediately after the first yield in most cases, so it can be deduced that the remaining strength is still stored inside the members until it totally dissipates at the ultimate state. The extra member capacity transcending the first yield is known as the inelastic reserve capacity. Experiments have shown that the inelastic reserve capacity of the sections is 20 – 75 percent greater than the first yielding capacity and adding stiffeners to the flange edges can be a more productive way of reducing the slenderness of thin-walled steel members than increasing their thickness (Baigent & Hancock, 1981).

### 2.3.6 Buckling behavior of CFS members with C-shaped cross sections

The C-shaped build-up section has one web and two flanges with light weight and small thickness, which may lead to various complicated buckling modes. As is noted by Lue et al. (2009), the subsequent failure mode of C-shaped sections can be affected by the

symmetry used. Doubly symmetrical cross sections may suffer from torsional buckling, while members with single symmetry build-up sections tend to behave more complicatedly under failure modes, which results in difficulty in classifying what kind of buckling modes are appearing in the member. As a result, buckling may occur on either the flanges or the web of a C-shaped cross-sectional member, which also requires researchers to take the residual stress and initial imperfections into account during buckling mode analysis.

The figure below indicates three examples of buckling modes which may occur in long C-shaped CFS members with lips, in which (a) represents local-plate buckling, (b) shows the distortional buckling mode, and (c) shows the flexural-torsional buckling mode shape.

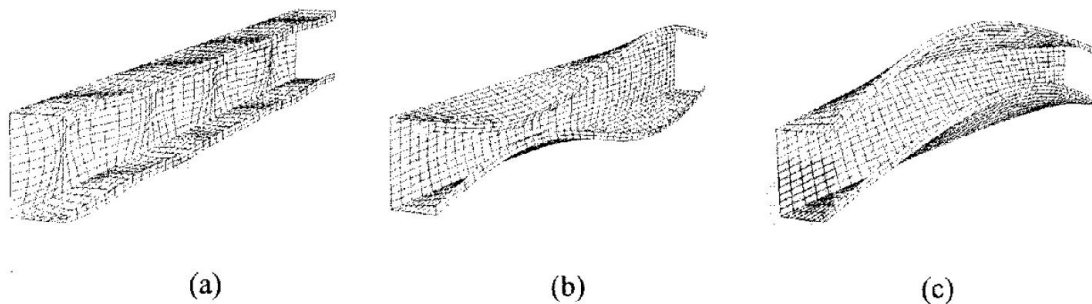


**Figure 7. Buckling patterns of C-shaped CFS members with lips (Camotim et al., 2005).**

#### 2.4 Cold-formed steel analysis

Structures composed of CFS members tend to have more complicated behaviour under axial and transverse forces, moments, and torques due to their integral shapes and material properties. The overall structural behaviours of the thin-walled steel structures under loading can be defined through the load-deformation curves shown in the figure, and each of the behaviours relates to a corresponding analysis method considering the real member response shown in Figure 8.

The thin-walled steel portal frame investigated in this research is supposed to sustain the wind loads from the lateral direction, and in its numerical model, the rafter and column ends are arranged orthogonally, and two 90° eaves brackets are deemed to be attached rigidly to the long beam rafter and columns at each corner, and the base joints are

designed to use rotation-free restraints at the nodes of each subdivided element at the bottom of the frame, and all the members and connections would be represented by Strand7 software.

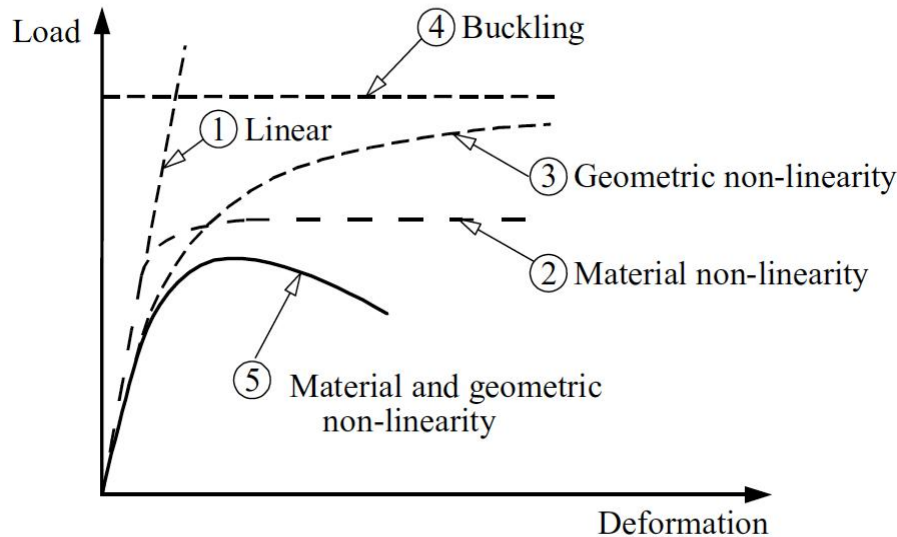


**Figure 8. Structure behavior of steel (Trahair et al., 1977).**

#### 2.4.1 First-order elastic analysis

Linear elastic response may occur on some materials with its load-deformation relationship curve drawn proportionally, which excluding the effects of the geometrical non-linearity and instability issues, as is shown in curve 1 in Figure 8. The deformations ( $\Delta_1$ ) are positively proportional to the applied loads ( $Q$ ) in the elastic equation shown below, where  $K$  is the stiffness matrix. And the superposition principle is applicable here to make the analysis easier (Trahair, 2012).

$$[K]\{\Delta_1\} = \{Q\} \quad (4)$$

In this equilibrium relationship, the stiffness affiliations are deduced with an unchanged profile of structures, so this analysis is restricted to tiny displacements (Rinchen, 2018). However, the C-shaped cold steel members investigated in this research have generally low toughness and high ductility, which could have an apparent displacement under the applied lateral load, so the first-order elastic analysis may not be valid to apply under the unstable condition of CFS. In this research, the first-order elastic analysis method would be used to test the accuracy of the numerical model to see if the modelling computing can operate smoothly.

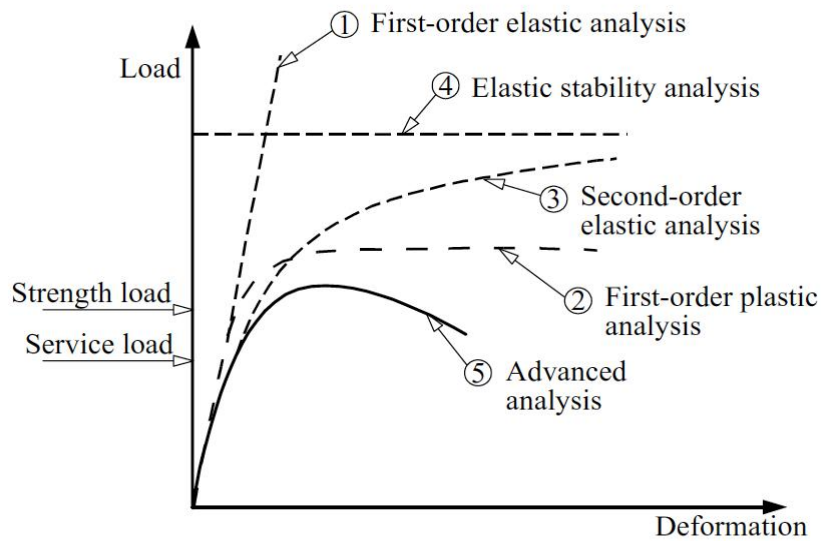


Figure 9. Possible curve shapes of different analysis methods (Trahair et al., 1977).

#### 2.4.2 Elastic buckling analysis

Elastic buckling analysis anticipates the failure mode under a branching equilibrium condition where the structure is expected to react perfectly under the increasing load, which indicates that no lateral deformation appears in the structure until the load reaches the critical amount. This condition can be explained by both curve 4 in Figure 8 and Figure 9, where the deformation data remains zero while the load is climbing to the critical load, then the deformation occurs and extends infinitely after the critical load.

Since first-elastic analysis does not help to anticipate the internal force responses and the deflection of a structure exactly when instability shows, elastic buckling analysis can bridge the gap in some way by applying the formula below (Trahair, 2012):

$$\{\Delta_b\}^T [K - \lambda_0 G] \{\Delta_b\} = 0 \quad (5)$$

in which  $\lambda_0$  is the buckling load factor and  $[G]$  is the stability matrix for the initial forces.

The linear elastic buckling analysis deduces the buckling loads under a relatively idealised assumption that the transformation before bending, the primary geometry imperfection, and the material nonlinearity are not considered in the analysis, which makes this method less

feasible in this research. And the buckling load concluded from this method is still different from that given by the Advanced Analysis.

However, the elastic buckling analysis is functional when the buckling shape result is used for representing the imperfection, and the effects are notable, especially in thin-walled sections (Rinchen, 2018). The buckling load factor  $\{\lambda_0\}$  derived from the elastic buckling analysis can be used to amplify the deflections produced by the first order elastic analysis. So that (Trahair, 2012):

$$\{\Delta_{1a}\} = \{\Delta_1\} [1-1/\lambda_0] \quad (6)$$

where  $\{\Delta_{1a}\}$  is the amplified result, while  $\Delta_1$  is the deformation results got from the first-order elastic analysis.

### 2.4.3 Second-order elastic analysis

The second-order elastic analysis is also known as Geometric Nonlinear Analysis (GNA), as the relevant equilibrium equations are developed by taking the geometrical deformation of the structure into consideration, but the material nonlinearity is exempted, which means the material is deemed to be linearly elastic. The performance of the structure under the second-order elastic analysis can be predicted by the curve 3 in Figure 8. A formula is designed to calculate the allowance for the establishing effect of higher accuracy (Trahair, 2012):

$$[K-G]\{\Delta_2\} = \{Q\} \quad (7)$$

In which the applied loads are equal to the the difference of stiffness matrix and stability matrix timing the structural deflection ( $\Delta_2$ ) under the second-order elastic analysis, which represents that the deformation of geometry is considered to weaken the stability of the structure.

In this analysis, the approximate results of the geometrical imperfection can by approached with the equivalent geometric imperfection,  $\Delta_i$ , and the shape of the imperfection is the one got from the lowest elastic buckling mode  $\Delta_b$ , which is further scaled by the scaling factor  $\alpha_i$  provided in the standards (Trahair, 2012):

$$\{\Delta_i\} = \alpha_i \{\Delta_b\} \quad (8)$$

To present the equivalent imperfections conveniently using statistics, equivalent loads are usually applied to make a substitution, where  $Q_i = K \Delta_i$ . Then the equilibrium Equation 8 is improved by adding the consideration of converted-to-load imperfections, whence:

$$[K-G]\{\Delta_{2i}\} = \{Q + Q_i\} \quad (9)$$

Since the deflected shape of the structure is not possible to predict beforehand and varies continuously during loading, an iterative method is required to form a gradually generated force-displacement relationship with designed load increments. In fact, this nonlinear analysis has an approximate result derived from a round of linear analyses when each load increment is applied. So, during each iteration, both external and internal force balance should be reached, and the stiffness matrix is renewed at each load step as a result of the related update of the frame changing from the last solution.

As the design concept of CFS sections is to use the benefits of various cross-sectional shapes to optimise the load capacity and reduce the manufacture costs (Cheng, 2005), the nonlinear deformations in the configuration may occur at an early stage and account a lot for the formation process, the final pattern of the load-displacement curve, and the load capacity limitation of the investigated CFS portal frame.

Moreover, in this research, due to the special material property of the CFS, the material nonlinearity still plays a part during the plastic deflection age as the lateral load is being added to the frame. So material nonlinearity is also taken into consideration in this article.

#### 2.4.4 Plastic analysis

The plastic analysis method aims to detect the ultimate loads of a steel structure, which lead to the failure of the whole structure due to the building up of over-displacement (Neal, 1977). Compared with other elastic analysis methods, plastic analysis helps design structures of relatively low costs and makes the structural analysis easier.

Three main assumptions are indicated to comply while using the plastic analysis methods, which are ductile steel structures, decisive design criteria excluding large deformations, and no local or global buckling before collapse loads (Qing, 2015). So in the plastic analysis, the detected steel frame is assumed to have no buckling appearing during the elastic stage and the

following plastic stage while the loads are being added until the whole structure fails, and the load capacity would only be caught at the plastic stage.

From the concepts above, it can be found that plastic analysis is only applicable to structures having tiny axial forces and instability impacts. However, as to the thin-walled steel portal frame explored in this research, the thin members tend to suffer from apparent instabilities and bulking in an early elastic stage, so the plastic analysis may be less relevant to the regular structure design built by cold-formed structures.

#### 2.4.5 Advanced Analysis

The Advanced Analysis is a computer-based approach to assessing the system and member strength and the stability of the whole structure directly, which means separate checks on the capacity of each member can be omitted. The reason behind the relatively simplified analysis process is that the Advanced Analysis takes the material and geometric nonlinearity into account in a straight way (Wai-Fah Chen & Kim, 1997). The strength and stability limitations of an overall structure and each component can be obtained efficiently and competently using Advanced Analysis, which distinguishes it from other traditional analysis methods. The behaviour curve of steel structures analysed by the Advanced Analysis is shown in Figure 9 curve 5.

As is mentioned before, the two significant characters related to the stability performance most, the material and geometry nonlinearities, together with imperfections, are included in the Advanced Analysis as essential considerations. The material nonlinearity causes progressively yielding of the composed members affected by the residual stresses and flexure. While the geometric nonlinearity is consistent with second-order effects concerning load-stress and load-displacement effects as well as geometric imperfections (Kim & Chen, 1999). Geometric imperfections are usually divided into three types, which depend on which part of a frame they occur in and their occurrence forms, namely frame imperfections, member imperfections, and sectional imperfections (Sena Cardoso & Rasmussen, 2016).

The advanced analysis, which is based on second-order elastic analysis, is also a type of nonlinear analysis, consisting of segmented linear analysis in small time steps using either load increments or displacement method, and at each time step the static equilibrium is maintained by iterations through the operation of several nonlinear algorithms, each of which

provides the same approach. To fulfil the equilibrium situation during each segmented linear analysis, the step length of the force increase or displacement increase is controlled. Either controlled method is chosen according to the prediction from researchers about the possible behavior of the structures. If the displacement reaction increases continuously with the simultaneous load increment, the force-controlled method would be used. In another way, if the response is progressively softer after the peak load is reached, displacement control is required to push the solution beyond the maximum point on the load-deflection curve. There is also a case where the structure suddenly breaks and reaches equilibrium in a different configuration, as is the case in the fracture problem (Rinchen, 2018). Due to this special way of detecting the structural stability in the Advanced Analysis, the load-displacement curve is formed in a gradual and continuously changing way depending upon the structural responses under each load or displacement increment during each iteration.

According to the detailed explanation from Torkamani and Sonmez (2008) about the two types of variation controlled nonlinear analysis methods, one of the most robust and popular strategy adopted to solve the nonlinear problems is Newton-Raphson technique. In this technique, the load incremental parameters is controlled to be zero ( $\lambda_j^i, j > 2$ ) during all the iterations except for the first one ( $\lambda_1^i, j = 1$ ), which is defined to 1. The first iteration has almost the same procedure as that in linear incremental analysis. But at the end of the first iteration, the calculated member forces are represented using global coordinates, and after that the unbalanced load factor coming from the imposed external loads and internal node loads would be decided.

In the meanwhile of the following iteration process, a planned convergence value is set to be contented, which can also be categorized into a load based one and a displacement based one, where the former one (Equation 10) is defined as ratio of the imbalanced load to the incremental force and the later one (Equation 11) is set to be the ratio of the first iteration to the last iteration deflection values.

$$\epsilon_R = \frac{\|\{R_j^i\}\|}{\|\{\Delta F\}\|} \quad (10)$$

$$\epsilon_R = \frac{\|\{\Delta U_j^i\}\|}{\|\{\Delta u_1^i\}\|} \quad (11)$$

The other method, contrary to the Newton-Raphson technique, is the displacement-controlled method, where the iterations are operated under consistent displacement increases in order to determine the corresponding load accumulation. This method is able to draw the load-displacement curve beyond the load limit point, but it is more suitable for analysing small structures or those that have structural behaviour people are familiar with.

The improvement of speedy desktop computers and concurrent computational devices allows completely nonlinear Advanced Analysis to be applied to large structural systems at a speed that can be used for conventional structural design. Also, the Advanced Analysis can help analyse complicated structural behaviour in a detailed way for research objectives (Rinchen et al., 2019). The computer software can detect the equilibrium situation of the structural system by imposing the incremental load on it during each piecewise step and give judgments on whether the load-displacement can be drawn under this step subsequently according to the reaction of the structure to that incremental load.

In this research, the finite element software Strand7 is used to apply the statistics for nonlinear analysis to the research subject. The analysis method used for this research may be a little different from the exact Advanced Analysis, as the initial geometry imperfection is excluded from consideration factors. It is supposed that no errors like slight deflections and rotations would appear in the frame and members during the installation process. Also, the initial deformations of the cross-sectional shape are neglected as no other loads are imposed on the frame model until the load increment begins.

## **2.5 Cold-formed steel portal frames**

CFS members can be used to create light-weight structures of large spaces without great material consumption and cost, and portal frames are one of the most popular construction forms. Steel portal frames are usually composed of columns, rafters, apex and eave joints, base connections, and so on. The structure of portal frames provides a large space for single-story constructions like residential houses, warehouses, garages, and workshops. In all forms of portal frame buildings, single-span portal frames are the most popular due to their relatively easy method of construction (Rinchen & Rasmussen, 2020). CFS members have gained great popularity in the construction of low-rise buildings. Also, for portal frame buildings, which are traditionally built with hot-rolled steel sections, CFS sections can work as an alternative with a span up to 20 m (Phan et al., 2017, Dundu, 2011).

Although the benefits of CFS portal frames, like decreased cost in the delivery process and on-site composition, are acknowledged by people when they choose to replace hot-rolled steel portal frames with cold-formed ones, the thin-walled steel always suffers from various types of instabilities, and comprehensive analysis of the whole structure is required. Luckily, an accurate prediction of the strength behaviour can be acquired with the help of finite element models and nonlinear analysis methods.

Many research studies on CFS portal frames chose to make the structure tougher by using an apex or by using sections which combine two single cross-sectional members face to face or back to back together. Those methods can efficiently raise the load-bearing capacity for CFS portal frames, but connection elements like bolts and fasteners are also required in high amounts, and welding may also be needed to connect adjacent members tighter, which adds cost for construction and refutes the aim of this research. However, some studies used simple CFS portal frames without too many reinforcement measures to test their strength behavior, which was found to have something in common with this research. As such this section will introduce several studies that use finite element models and nonlinear static analysis to investigate cold-formed portal frames. The details of the modelling process would be contained together with the efficiency of the numerical analysis.

Zhang et al. (2015) used 4-noded general purpose shell elements with reduced integration (S4R) in Abaqus to model the back-to-back connected double C-section pitched roof portal frame tested in their earlier experiment. The aim of building finite element models was to display the use of the stiffness-based beam element method in portal frames, where local/distortional buckling modes were taken into account. The method was fulfilled by declining the member stiffness in the context that the frames were being put under load and deforming consequently. The numerical models were built with the same strength performance as the tested portal frames, which were designed with rather slender cross sections, and the early-edge large instability behaviour was guaranteed to occur. The mesh size in the plate sections was set to be approximately 25×25 mm after convergence studies. Moreover, to make sure that the portal frame deformed in a single 2D plane, discontinuous restrains were attached to avoid lateral and torsional deflections out of the plane. The apex angle of the portal frame is 152° and the original structure elevation used for both the experiment and the FEM is shown in Figure 10.

In the modelling process, the joints at the apex and eaves were designed to be semi-rigid with overlapping rotational spring elements arranged at the centre of the joints. The length of the rotational spring elements was neglected, which also indicated that coincident points on the respective members were ready to be connected. As to the contact elements for the back-to-back double-C section members like rafters and columns, fasteners were not modelled in detail as to their physical configurations. Surface-based contacts were defined, however, by selecting different functions for the backs of the webs on the corresponding single C-section members in Abaqus. By defining the contact normal behaviour as "hard" and the tangential behaviour as "rough", penetration and slide were avoided between the two fitted member surfaces. These two functions were considered adequate to simulate the behaviour of fasteners during modeling, and the back-to-back members thus got a complete combination across the contact area. However, if the gaps between webs were larger than 6 mm, like the joint area where brackets were inserted between the two webs, fasteners were built into shell models together with "tie" restrains in between surfaces of webs and brackets.

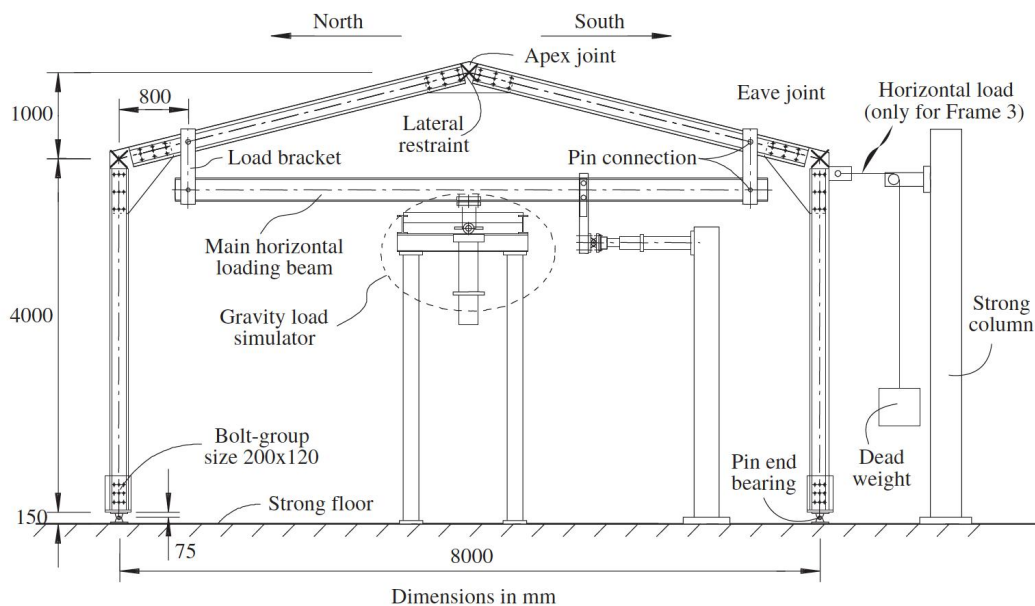


**Figure 10. Back-to-back double C-section Portal frame for experiment (Zhang et al., 2015)**

The geometrical and material nonlinear shell finite element analyses were conducted on the portal frame. Simple vertical and horizontal loading, as well as combination loads, were applied to the frame models. As is concluded from the numerical analysis results, the load-displacement curves obtained from each part of the portal frames went well with the results

from experiment tests, with the ultimate vertical loads reaching around 80 KN and around 5 mm of horizontal deflection found at the end of the elastic stage. Local buckling was found in the portal frame columns at an early stage when the applied load reached approximately half the value of the ultimate load, while distortional buckling appeared later when the applied loads almost reached the ultimate loads. The failure of all the finite shell element frames was mainly attributed to the development of structural plastic mechanisms in space. Moreover, it was also found that the ultimate load may be overestimated if the original local and distortional buckling imperfection was neglected.

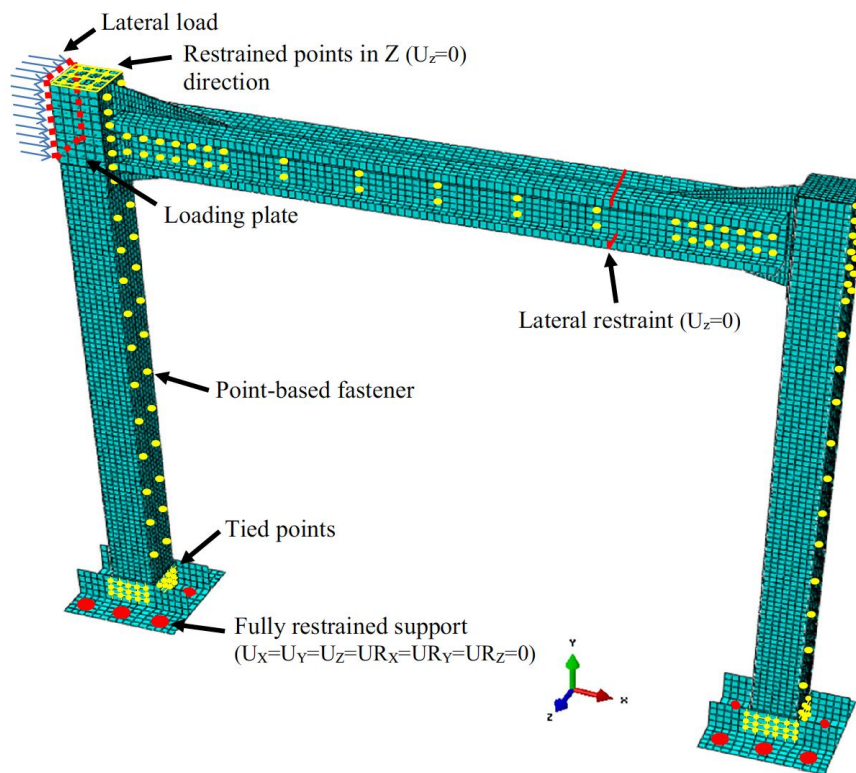


**Figure 11. Finite element model for lateral load resistant portal frame (Mojtabaei et al., 2018)**

Mojtabaei et al. (2018) used a half-scale CFS portal frame to test its seismic performance under monotonic lateral loading. The design theory of the portal frame involved composing rough columns and weak beams by rigid moment-resisting connections. The columns were built by using two face-to-face C-section members bolted with inner plates along opposite flanges to make the cross section a box shape, while the beams were constructed using back-to-back connected C-shaped channel members with gusset plates bolted on either

end. The base connections were designed to be rigid by applying hot-rolled angles. Also, a finite element portal frame model using SR4 elements in Abaqus was built consistent with the primary components described above. The numerical model was designed to simulate the strength performance of the tested portal frame, which is shown in Figure 11. During the modelling process, an element size of 15×15mm was found most efficient to derive accurate results, and the geometry imperfections and material nonlinearity were taken into account.

The material nonlinearity was considered by using the Ramberg-Osgood stress-strain relationship to determine the stress-strain curve for the material. As to the geometrical imperfections, the eigenvalue elastic buckling analysis in Abaqus was used to find the first buckling mode for the portal frame, which could be adopted as the typical patterns of local and distortional imperfections.

For the rather detailed connection parts in the finite element model, point-based "fastener" elements were applied at the same location as the bolt groups to connect beam and column elements with the gusset plates, and bolt slippage was avoided by applying "BEAM" connector elements on fasteners. Also, the base angle connection was fully restrained by using the "Tie" command. At the lateral loading area, discrete rigid shell elements were used to model the thick load plate in the laboratory test at the left top joint area shown in Figure 11, and lateral restrains were arranged along the beam to prevent out-of-plate deformation.



**Figure 12. Finite element model for tested portal frames (Rinchen & Rasmussen, 2019)**

The result of the nonlinear finite element portal frame was validated by the test results from experiments. Comparable results were found in either experiment method with a similar value of lateral displacement (86 mm) occurring during the material elastic stage as the loading was adding the largest capacity value gradually (FE model: 39.48 kN, Experiment: 38.14 kN). The main failure mode was detected to appear locally at the bottom and top of the columns, mostly blaming the web crippling.

Rinchen and Rasmussen (2019) built a numerical model using Abaqus for the portal frames, which were tested in their previous experiment to explore the strength behaviour of the single C-section portal frames. The elevation together with the 3D model of the whole tested portal frame structure are shown in Figure 13 and Figure 12 respectively.

As is shown in figure 12, the two end frames were built by double C-section members connected back-to-back, working as elastic constraints for purlins arranged on the middle single C-section portal frame, which helped better simulate the realistic loading conditions and the load transfer forms for the single C-section portal frame located in the middle.

Figure 13 gives the dimensions of each part in the portal frames, in which models of rafters and columns were built separately and arranged on the relevant bracket, and the base boundary conditions were set to be semi-rigid due to the flexible joint fittings present on the base. The apex angle is  $160^\circ$  with rafters tilting  $10^\circ$  downwards horizontally on the opposite side. As to the connections between each element of the portal frames, it is worth mentioning that mesh-independent point-based fasteners were applied to function as idealised bolts and screws at their physical locations. A validation test was also carried out for the fasteners by modelling the slip-resistant point fastener shear connection tests in the experiment, and the numerical modelling results showed a high level of agreement with those received from laboratory tests.

The columns and rafters were built by extruding the cross-section profile along the longitudinal direction of a proposed member using 4-noded shell elements, S4R. The major mesh dimension for the portal frame is 15x15 mm, while mesh sizes in elements which require additional detailed modelling vary with the corresponding desired shapes.

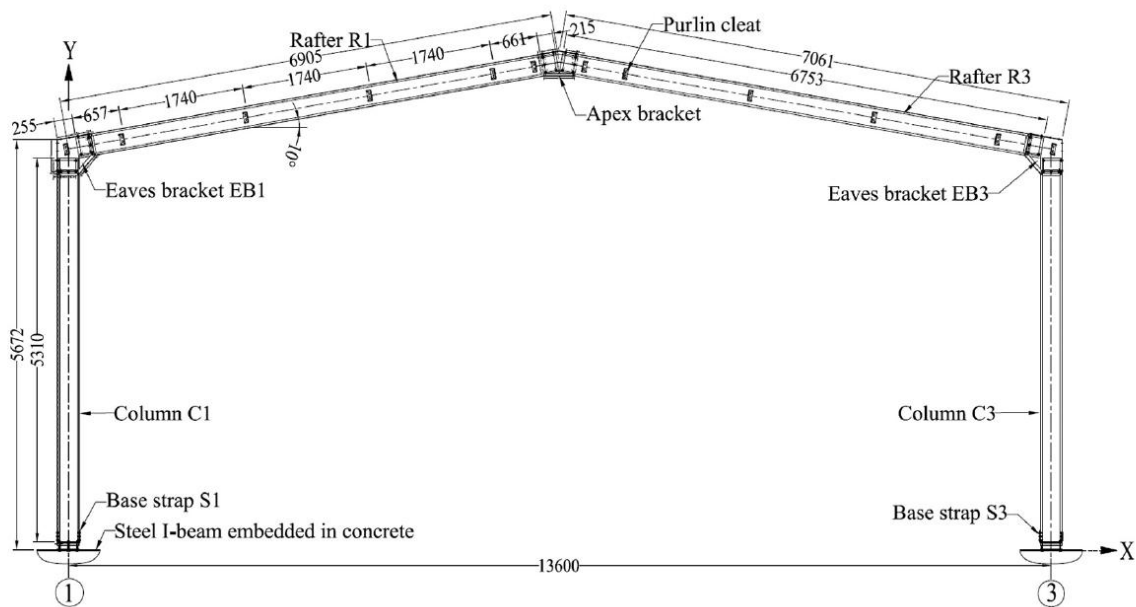


**Figure 13. elevation of single C-section portal frame (Rinchen & Rasmussen, 2019)**

A nonlinear static analysis considering both geometry and material nonlinearity was applied to the frame modal, and 6 tests were carried out with various load steps chosen for different vertical and horizontal load combinations exerted on the models to follow the same condition in the experimental tests. The final results showed that almost all the ultimate loads from each frame element obtained from the Advanced Analysis were in good agreement with those obtained from experimental tests, and flexural-torsional buckling is the primary deflection mode for single C-section portal frames without lateral restraints attached to the frames. Solutions to this problem were provided by the researchers to reduce the twist behaviour of columns by attaching girts directly to the column web.

## 2.6 Summary of literature review and the research gap

To conclude from the literature review above, the strength behavior of the CFS is described with reference to its stress-strain curve of a rather plain yielding plateau. Due to the mono-symmetrical geometry of the C-shaped cross section, twist behavior may occur if the load is the eccentric. Additionally, member warping and web crippling together with various modes of buckling would occur on a loaded CFS attributed to the instability behavior in the thin-walled section. Much research has been done to explore the vertical and horizontal load resistant performance by computational modeling for CFS members and structures, from single member sections to portal frames, shear wall panels and multistory rack structures.

Also, nonlinear analysis considering both geometry and material nonlinearity using finite element model is proved to be efficient for exploring the strength behavior on a structure which keeps deforming.

CFS portal frames are recently of high popularity and are being explored as an alternative to substitute the load resistance use of hot-rolled steel frames in low-rise buildings. It is also the aim of this research to replace the hot-rolled parallel C-section frames in residential buildings with cold-formed ones, which is estimated to further decrease the construction costs and make the construction more effective. However, almost all the portal frames detected have used apexes and declined degrees along the rafters. These kinds of portal frames may not be suitable to be inserted into a residential house to work as its main transverse force-bearing and weight-loading frames on the ground floor. An inclined roof between stories adds difficulty to upper floor construction and creates more unapproachable spaces between floor partitions. In the meanwhile, much research has been done on the CFS structure cross sections having two single cross sections combined to fulfill a larger cross-sectional area in order to provide higher stiffness for the composed member, but the exploration of the single C-sectional CFS portal frames is limited due to the susceptible strength behavior. The previous tests on the lateral resistant strength of a portal frame mainly applied equivalent node force on one of the eave joints, which were not able to fully simulate the effects of distributed wind load required in residential construction. As a result, in this research, the lateral resistance performance of a single C-shaped cross section cold-formed portal frame with no apex angle (rectangular shape) will be investigated to determine its applicability working as a primary load resistant structure built inside a residential building. A detailed plate finite element model is made to simulate the strength behavior of the single C-shaped cross section cold-formed portal frame. Static nonlinear analysis will be operated on the finite element portal frame model using Strand7 software to explore the strength performance of the explored portal frame.

### **3 METHODOLOGY AND PORTAL FRAME MODELLING**

#### **3.1 Overview**

This research aims to make thin-walled steel residential construction more cost-effective by replacing the hot-rolled steel portal frame structural system in the residential houses with a

cold-formed one. To fill the research gap and detect whether the designed no-apex CFS portal frame is reliable to work as the major structural component in a low-rising residential house, a similar or scaled portal frame should be investigated through experiments to explore the strength performance. However, since it is not feasible to proceed with experimental tests due to the time and cost limit, in this research, a plate element finite element model is built to simulate the lateral resistant behaviour of the cold-formed single-C cross-section steel portal frame under wind loads. The overall dimension of the portal frame model is the same as the physical one, which is designed to be suitable for being installed in residential buildings. Also, full-scaled models can sufficiently provide precise analysis results from the intricate interactions between major frame members (Davies et al., 1990) and help identify which part of the structure is fragile and make precisely located improvements to the structure design (Blum & Rasmussen, 2019).

This research only focuses on the load-carrying capacity in the horizontal direction for the CFS portal frame, and the designed horizontal force mainly comes from the wind load. The finite element model is built by Strand7 Software using plate elements with rigid link elements working as idealised bolt connections to compose different frame elements together, and the Advanced Analysis method discussed in Chapter 2 is applied considering only the geometrical and material nonlinearity in the Strand7 solver. The geometrical imperfections are excluded from this research by assuming perfect initial conditions and an assembly process for the structure. The accuracy of the plate element model is validated by posing a node force on the left top corner point to see if there is the same value of overall reaction forces all over the model. The displacement reasonableness is validated by comparing the integral displacement distance and deformed shape of the plate element model with a beam element model of the same configuration under a same node force. The validation process for the force reaction performance of rigid link elements is also included using FEM analysis. All the validation tests, including reaction, displacement, and rigid link elements applicability tests, are conducted through linear static analysis using the coarse meshed model in the Strand7 solver.

### **3.2 Theoretical base**

The thin-walled steel is a ductile material notable for large deformations and various early-edge buckling modes, and the single-C shaped cross-section is more susceptible to eccentric

forces, as is mentioned in Chapter 2. As a result of this, the static nonlinear analysis method including geometry and material nonlinearity was selected to be used for this research, as the completely nonlinear analysis has proved to be available for reflecting the behaviour of steel structures in a set of buckling modes with high accuracy (Sena Cardoso et al., 2019). As a result, the structure is analysed based on the deformed shape of the previous step after the first load increment, which also considers stiffness degradation of the yielding material and residual stress effects. The Newton-Raphson technique mentioned in Chapter 2 using controlled load steps is applied in the nonlinear analysis by putting orderly growing load increment factors in the Strand7 setting. So the horizontal distributed face load is applied to the frame progressively in load increments, which has increasingly multiplied values of the initially applied force. During the calculation process in each load step, the software will automatically choose the suitable number of iterations. Initial geometry imperfections caused by manufacture deficiencies and assembly faults are excluded from the nonlinear analysis in this research. During the modelling process, bolts were replaced by rigid link elements in Strand7, and the inspiration gained from the FEM mentioned in Chapter 2: 2.5 section, where other researchers use valid node connection elements in modelling software to substitute the modelling of real-configured bolts.

### **3.3 Finite element modeling**

#### **3.3.1 Modeling approaches**

A finite element model was built using plate elements in Strand7 software, and it has a full-scale dimension of the portal frame which is supposed to be used in residential building construction. Figure 14 shows the global shape of the cold-formed steel portal frame, which has an overall height of 2.8 m and a span of 3.2 m considering the structure thickness and spacing between different frame elements.

In the portal frame, each element, namely columns, the beam, eave brackets, and base plates, was modelled by coordinating their cross-section location points along the centerline of the plate thickness. This means that the plates get thicker along with the opposite vertical directions of the centreline when Strand7 software assigns thickness to the plate elements. The mono-symmetrical cross-section shape is shown in Figure 15. The column members and the beam member all have the same C-shaped built-up profiles with two 28 mm lips ( $L = 28$

mm in Figure 15), while the eaves brackets have no lip ( $L = 0$ ) with bigger cross-sections in order to locate other members inside.

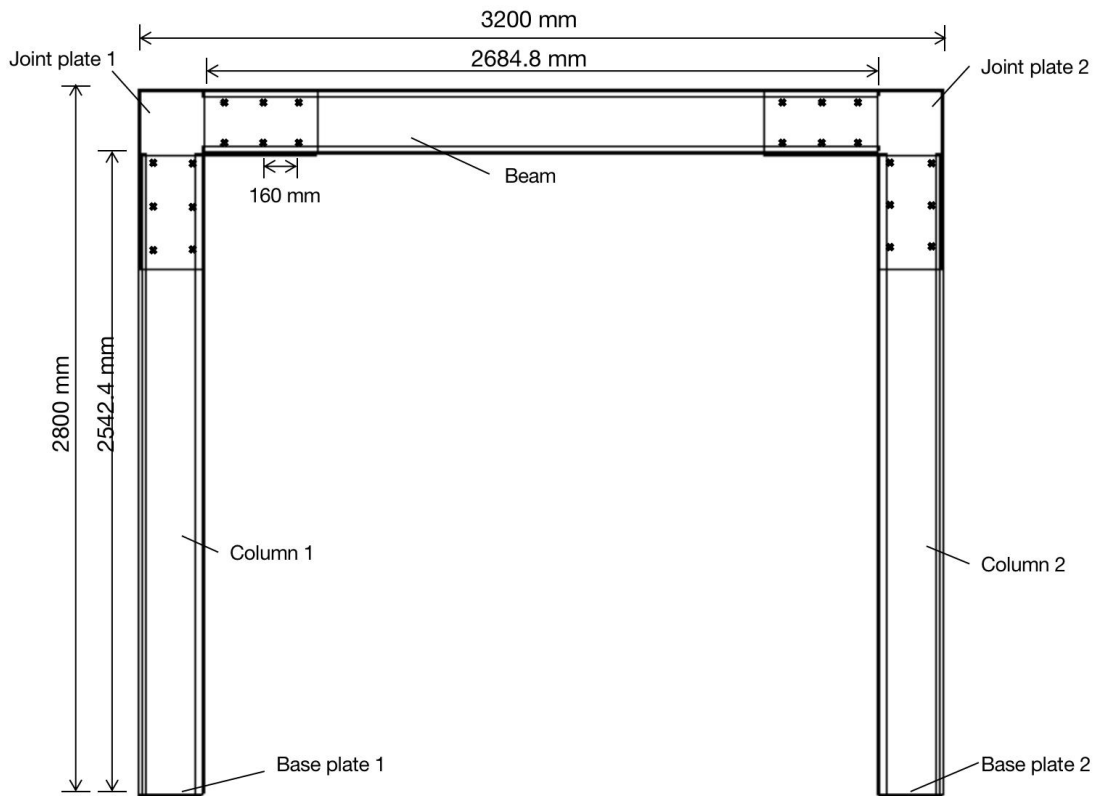


**Figure 14. C-shaped cross sectional CFS portal frame model sketch with dimensions**

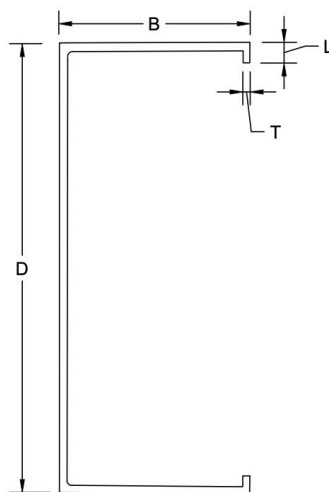


**Figure 15. Cross section dimension drawing**

For column and beam members, the length of the flange, which is represented as B in Figure 15, is 70 mm, and the web is 250 mm in width. In eaves brackets, the edge of the joint plate (B) is 72 mm and the width (D) is 258.8 mm. In the portal frame, the eave brackets semi-wrap the ends of columns and beams with a 2 mm gap and are bolted on the web of the member ends with the same opening orientation as the C-shaped section. The thickness (T) of all the plate components is 2.4 mm, except for that of the base plates, which is 8 mm.

The detailed dimensions of the joint part can be seen in Figure 16. Groups of bolts are supposed to be used for the connection parts where two plates are stacked on the top corners. In the finite element model, rigid link elements were applied to connect different elements of the portal frames, and verification of the link efficiency is discussed in this article. In Strand7, rigid link elements are defined as a link connection between two nodes with infinite stiffness, which can prevent any relative displacement and rotation between the two selected nodes sufficiently.

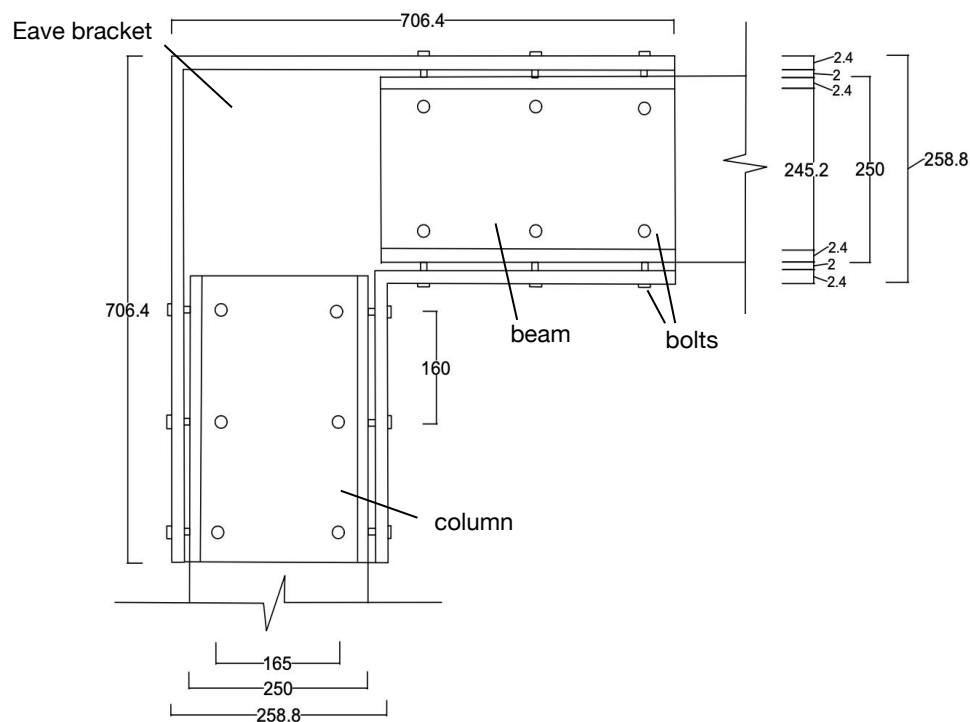


**Figure 16. Eave joints components**

For each group of bolts at the connected part of two stacking plates, rigid link elements were used to link the nearest mesh nodes on each plate at the approximate location of the real bolts.

The biggest distance among all linked couple nodes is 10 mm horizontally and 4 mm vertically. A total of 48 rigid link elements were assigned to the frame model, with 2 groups of 6 rigid link elements connecting the webs of the beam and the eaves brackets, 2 groups of 6 rigid link elements connecting the column webs and the eaves brackets on each side, and 4 other groups of 6 links used to combine the flanges of different components at the locations directly opposite to those of the web-bracket connecting links, which is aimed to avoid plate alignments and crossings under large deformations. So all the links were applied to make various components combine as a whole and deflect integrally.

Figure 17 gives an overview of the finite element model with the coarse mesh. The middle beam, two columns and two right angle joint plates were extruded from beam element cross sections along the longitudinal direction of the member using Quad 4 plate elements in Strand7. The base plates were built by connecting the cross section coordinate nodes into closed rectangle plates and further subdivided into proper sized Quad 4 elements.

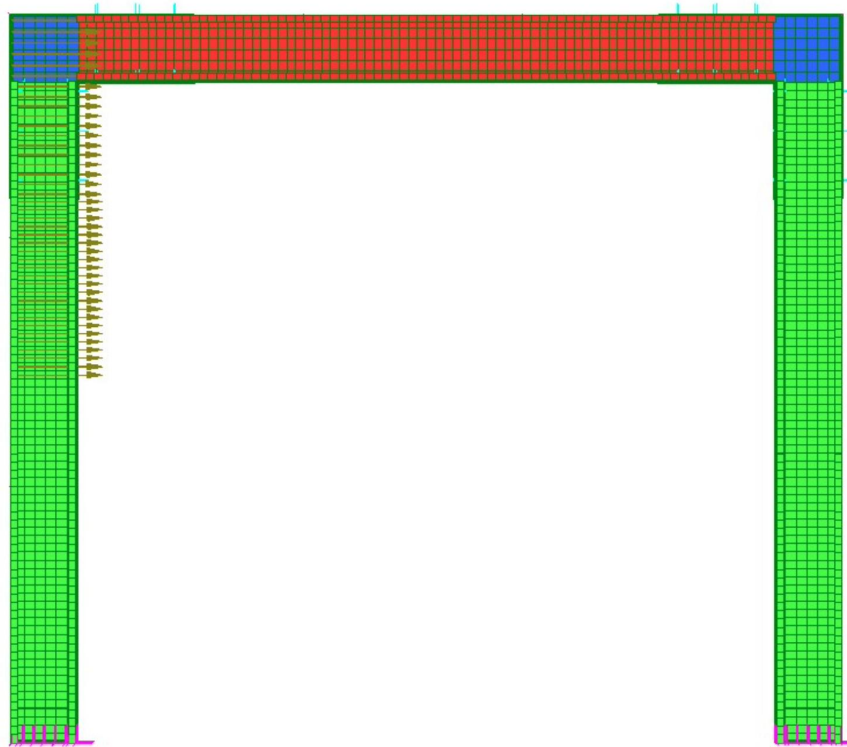


**Figure 17. Finite element model for the CFS portal frame using C-shaped sections**

Quad 4 elements represents 4 node quadrilateral elements, which have linear shape functions with always straight boards under global structure deformations. In each element, the

stiffness of the material is deemed to be infinite, as the mesh size is rather small compared with global frame deflections. So the shape changing of each small element is defined as linear and all the tiny linear deformed element plates work together to form a comprehensive and curved deflection shape for the whole frame structure. As a result of this, Quad 4 elements are assumed to be able to function efficiently during modeling and analysis process and make the solution easier. As to the frame dimensions, especially the frame height, were determined by the maximum peripheral dimension of the joint plate sections, the length of all the members tend not to be integer numbers. So the mesh sizes in different components of the frame structure were set under an idea that the total amount of mesh in a member is an integer and all the elements are complete. The coarse mesh of an average size of 40×40mm was applied in the first trial to verify the function accuracy of the portal frame model and give out an overview of the structure strength under supposed loads. Further convergence studies were carried on models of mesh sizes of approximately 20×20mm and 10×10mm.

The material used in the finite element model is "steel" of structural steel in the Strand7 material library, with the Young's modulus of 200,000 MPa, Poisson's ratio of 0.25 and a density of  $7.87 \times 10^{-6}$  kg/mm<sup>3</sup>. By inserting the material properties into the Strand7 static nonlinear solver setting, the stress-strain curve is not needed to define using the data from the coupon test especially.

As to the boundary conditions of the finite element portal frame model, all the nodes at the base plates were restrained with free rotations and fixed translations. In real construction, two side-by-side rivets are nailed through the base support gusset into the concrete basement on the ground, which can prevent rotation in all directions and allow in-plane translation. Furthermore, because the wall and floor panels installed around the load-bearing portal frame prevent out-of-plane displacement, lateral restraints with no translation out of the main axis plane were added discretely along the frame members, with two at the opposite top frame corners, two along each column, and another two along the beam at an average distance.

An initial horizontal wind load of 0.01 MPa was applied as face distributed loads on the lateral side of the upper half part of the frame, and all the loads were located on the outer flange surface of the left joint plate and the column. The structure is supposed to sustain a total of 0.06 MPa of lateral wind load under the commonly used requirement of residential housing construction, which specifies that every 3 m long lateral wall needs to sustain a 1.4

KN/m<sup>2</sup> designed wind load. So, according to the width of the flanges along the loaded member, 0.06 Mpa is needed to apply to the flange along the upper half part of the left column. The whole structure is designed to sustain 20 times the wind load of approximately 1.2 MPa, considering the effects of bolt failure in realistic conditions. Because rigid link elements are applied in the finite element model, the whole portal frame model would deflect integrally when it is pushed by the wind load, and the results would reflect the stability of the portal frame regarding its material and structure. In reality, the bolts connect different portal frame components and need to sustain large shear forces to maintain the composition of the whole structure, to which contribute a lot to the final failure mechanism of the portal frame.

After several trails in the computer program, a load and freedom cases increment factor table was determined and shown in table 1. It was found that the frame underwent an elastic deformation stage during approximately 1-95 times the initial load, which meant that the frame started to deform nonlinearly after 0.95 MPa of face load and the frame began its plastic deformation after about 1.1 MPa. That is why the load increment factors began to increase little by little after 95 at designed intervals, and the load factors affected the curve shape visually to some degree during this deformation part. In the meantime, the curve shape changed finely during this elastic-plastic transitional phase and started to deform largely after 110 MPa. During the nonlinear analysis, the load scaling is selected for automatic sub-incrementation, which is suitable for stiffness-decreasing materials. Load scaling in Strand7 means that calculations for the current load increment would restart again with a half-scaled load factor if the result is not converged below the tolerance, and this procedure would repeat if the result of the sub-increment is not converged until the scaled load factor reaches the minimum limitation. The minimum reduction factor set for this static nonlinear analysis is 0.1 as default, and the displacement norm tolerance and the residual norm tolerance are set to be 0.001.

**Table 1. Load increments**

Step	1	2	3	4	5	6	7	8	9	10	11	12	13	14	15	16	17
Load factor	1	50	90	95	96	96.5	97	98	99	100	105	110	115	120	125	130	135
Freedom factor	1	1	1	1	1	1	1	1	1	1	1	1	1	1	1	1	1

### 3.3.2 Validation of rigid link elements

A finite element model containing two plates connected by a rigid link element in the middle is used to investigate whether rigid link elements can give a correct force reaction response in Strand7 to simulate the force behaviour of bolt connections. Figure 18 shows the different ingredients in the verification model.

In this model, two 80×80 mm Quad4 element meshed CFS plates with the same material properties as those in the investigated C section portal frame. Each plate was subdivided into 4 small plates of the same size. The upper plate was set to be 10 mm away from the lower plate in the horizontal direction and 4 mm away in the vertical direction. This relative distance between the two plates was determined by the biggest node distance in the portal frame model between two stacked components. The lower plate was constrained at all 4 corners with fixed translation only in the out-of-plane (XY) direction (Z direction), and a horizontal node force of 1N was applied to all the nodes, except for the connection node (node 7). All the corner nodes in the upper plate were fully fixed to simulate a single plate element in the portal frame. The rigid link elements were used to combine the two discrete plates by connecting node 10 and node 7 in the middle of each plate.

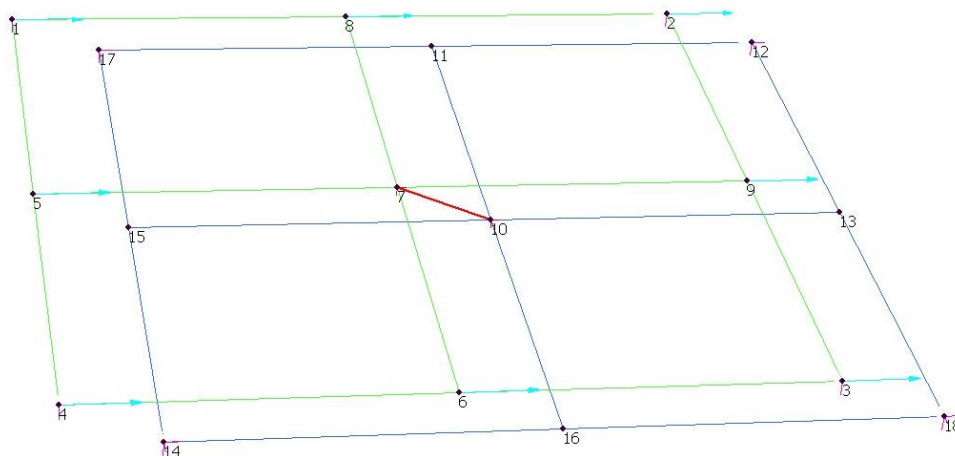


**Figure 18. Validation model for rigid link elements.**

After solving the model with the static linear solver, reaction forces along the horizontal direction were found in the 4 fully restrained corner nodes of the upper plate, and the total

value of the four reaction forces was found to be equal to that of all the node forces in the lower plate. The directions of the reaction loads were also contrary to the applied loads. So it can be concluded from the verification test that rigid link elements can perform efficiently when working as idealised bolt connections. Detailed horizontal reaction data is shown in Appendix for reference.

However, it is noted that rigid link elements have infinite stiffness, which is the reason that load increments could reach such a large value of 1.35 Mpa to form the whole load-displacement curve. In reality, bolt connections may already fail at 2.5 times wind load, which is 15 times the initial load, reaching approximately 0.15 MPa. Very slight displacement is also found within the nodes in this validation, which results from Quad4 element rotation and deflection under forces, since rigid link elements are infinitely stiffened.

### 3.3.3 Verification of the portal frame model accuracy

Force equilibrium validation was conducted on the finite element portal frame model to check if the structure is correct. The validation test was performed on the portal frame model of coarse mesh (40×40 mm) with a 10KN node force loaded on the middle point of the left bracket top corner, which is shown in Figure 19.

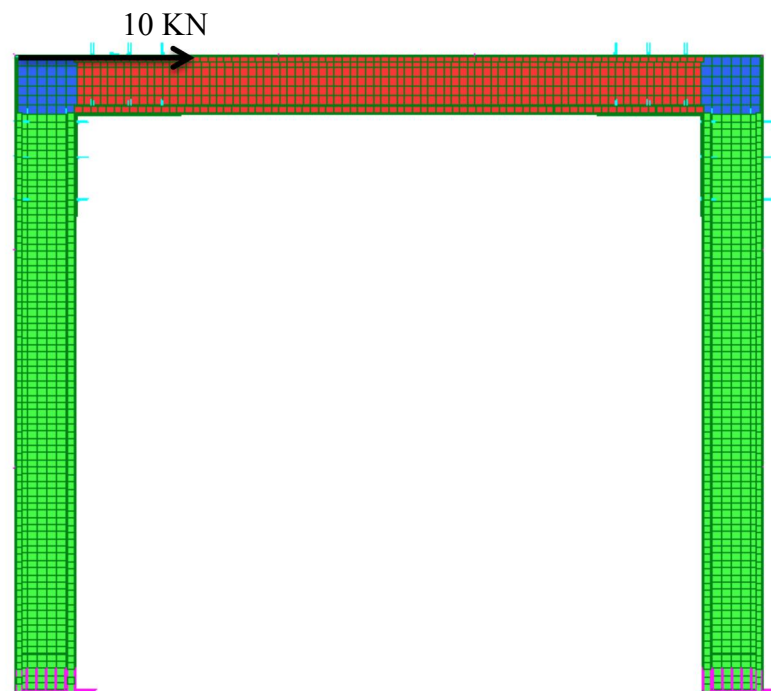


**Figure 19 . Force equilibrium validation model.**

A linear static analysis was applied to the model to test if all the horizontal reaction forces would balance the value of the external force. A total of 3861 node reaction forces in the horizontal direction (X direction) were exported from the result table and added together to find out if the total value was equal to the applied force. Results showed that the sum of all the support reactions was - 9999.999752N with the opposite direction of the external 10,000N force, which indicates that the portal frame performs well under external loads and can give correct results on forces.

Displacement validation was also conducted to see if the portal frame model deflected reasonably under lateral forces. To detect the validity of the displacement results from the Quad4 element model, a beam element model was built to make a comparison. The plate element model with the 40×40mm sized mesh was used for displacement verification. The location points of the beam ends in the beam element model were selected directly from the center lines of the members in the plate element model. The right-angle eave brackets were also built by two connected orthogonal beams. The properties and cross-section dimensions of the beams are similar to those in the plate model. The global size of the beam element model would be represented as the same in the plate model if all the beams are displayed as "solid" or "section" mode with a total span of 3200 mm and a height of 2800 mm. All the beam components in the beam element model were further subdivided along the members into the same number of beam elements as those along the members in the plate model.

As to the boundary condition, the beam element model has two fully fixed supports, referring to that all the nodes of the support plates in the plate element model were defined with free rotation and fixed translation, which can actually make the supports perform as fixed ones with mutual constraints from various simply supported nodes. Also, in addition to the base restraints, default freedom conditions, namely "2D frame" and "2D beam" in Strand7, were set for the plate model and the beam model, respectively. The applied 10KN node forces were also located at the same position on the left top of the centre line in both element models.

Static linear analysis was performed on the two portal frame models with different element types. The pictures showing the horizontal displacement conditions of both models in contour mode are attached in the Appendix. The result showed a maximum of 5.69 mm of deflection was found in the beam model and 5.22 mm was found in the plate model, which indicates

that the deflection result of the beam model was 9% smaller compared with the plate model. The main reason could be that the 2D plate element has more freedom degrees compared with the beam element, and the small result difference between the two types of models also gave credibility to the accuracy of the displacement in the Quad4 element models used for static nonlinear analysis.

### **3.4 Summary**

In summary, the finite element portal frame model was built to restore the real structure as far as possible, and the accuracy of the modelling analysis was also checked by validation models to make sure the final model can simulate the strength behaviour of the real structure functionally. Rigid link elements may increase the load-bearing capacity of the portal frame model, so further analysis considering the influence of real bolt capacity would be performed.

## **4 NUMERICAL ANALYSIS RESULTS**

In this part, distinctive results of different deformation stages are found from the static nonlinear analysis results, which were derived from CFS portal frame models with different mesh sizes. Three curves from different mesh refined models are compared together in Figure 20. Then a convergence study on the yield strength and ultimate strength data would be carried out. The curve with the most accurate result regarding the bond solution would be discussed in detail to define the different deflection phases with corresponding pictures of the critically deformed part. Then the capacity of the bolts would be analysed according to the support reaction forces to give an estimation of the true strength behaviour considering the effects of bolts in real construction.

### **4.1 Convergence study**

The portal frame was pushed by gradually increasing lateral distributed loads from 0.01 MPa to 1.35 MPa with respect to the load factor table in Table 1. Figure 20 shows a comparison of the load-displacement curve results among models with different numbers of plate elements and the models used idealised connections with infinite stiffness. Data derived from the static nonlinear analysis was used to depict the curve above, which is attached in the Appendix. The displacement data was selected from the maximum relative node displacement data between two typical nodes. One of the selected nodes has the largest horizontal deflection, which is located at the outer top point in the middle of the loaded left

eave bracket, and the reference point was selected from the lowest middle outer node of the left side support.

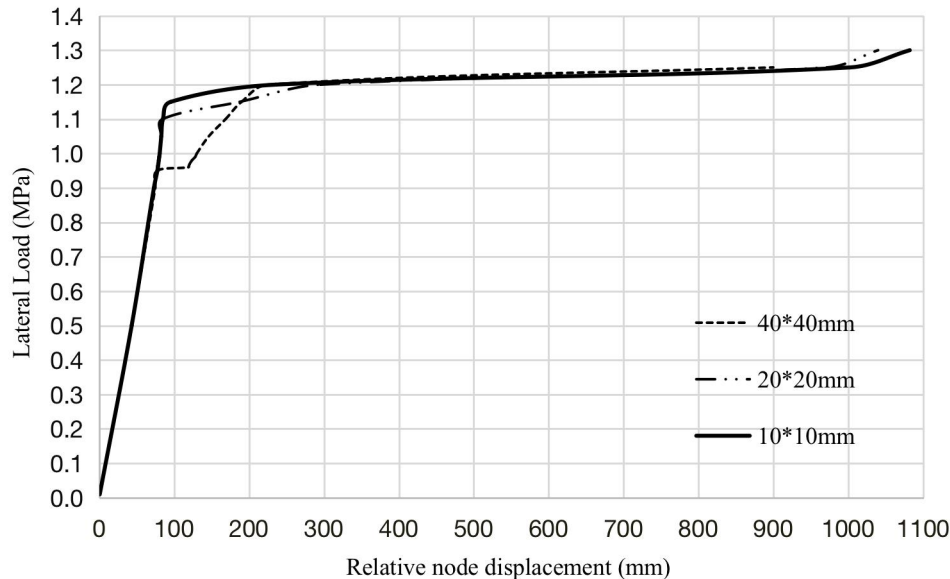


**Figure 20. Force-displacement relationship of portal frame models with different mesh sizes.**

The three curves have almost the same slope during the elastic deformation stage of the structure. Differences start to appear at the end of the proportion limits with different yield strengths captured among the three curves, and the trend shows that the derived yield strengths have a gradual upward tendency when the meshes get finer. The coarse meshed model undergoes a perfectly elastic stage with a large deflection of around 77 mm that occurs during a small load increment after 0.95 MPa applied load, while the other two finer meshed models continue to deform proportionally and reach higher yield strength at 1.1 MPa (20\*20 mm) and 1.15 MPa (10\*10 mm) respectively. Then the models with different mesh sizes all reached an ultimate strength of 1.2 MPa, excluding the effect of limited bolt capacity.

The convergence study is done by plotting the results of the yield strength with respect to the mesh numbers of the models. It is indicated in the figure that the yield strength converges to an upper bound solution of 1.15 MPa. The convergence plot demonstrates that fine sized mesh (10×10mm) can give out the most accurate data. But the calculation time was also prolonged by dividing the mesh into smaller dimensions. The graph shown in the figure gives the time consumption curve corresponding to the member sizes.

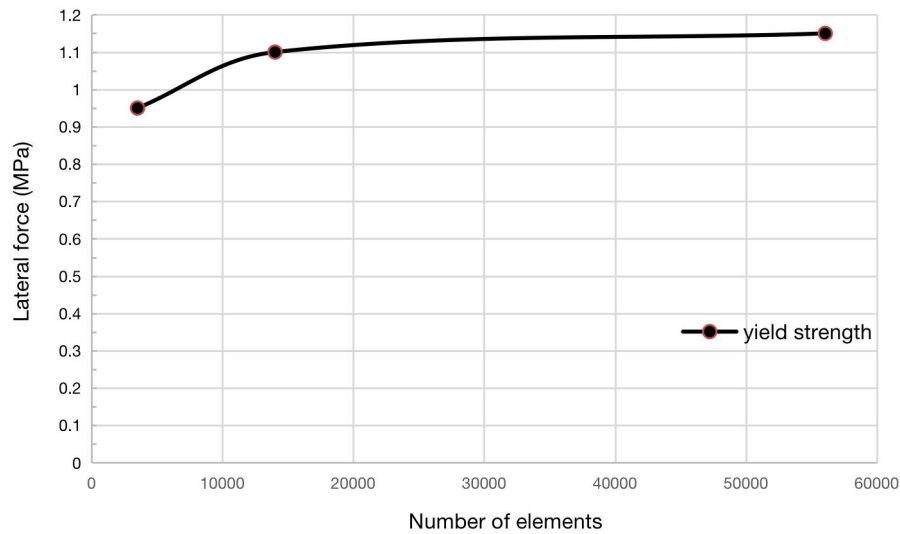


**Figure 21. Distribution of mesh sizes on the results**

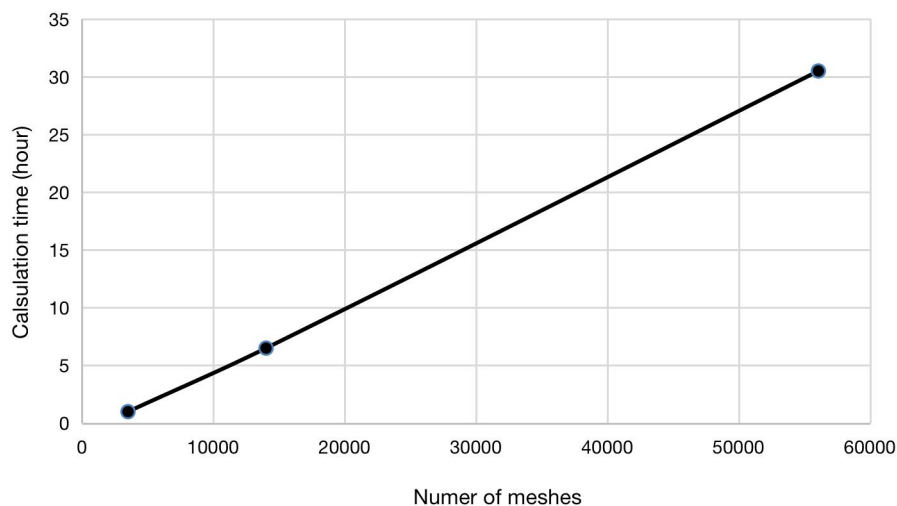


**Figure 22. Time consumption on the calculation**

#### **4.2 Load-displacement relationship and portal frame deformation shape**

Referring to the most accurate results from the fine meshed model, it can be concluded from the convergence study that the portal frame structure using the CFS material and the single C-shaped cross section shape has a yield strength of 1.15 MPa and can finally sustain an ultimate load of more than 1.2 MPa, excluding the effects of the early failed bolt connections. As is shown in Figure 20, while the portal frame works as a fully composed structure with the help of rigid link elements, the structure can deform elastically when the load is gradually increased from 0.01 MPa to 1.15 MPa, with the maximum horizontal deflection reaching more than 95 mm. Then the portal frame shows an ultimate strength of 1.2 MPa in the plastic

phase. The single C-section CFS portal frame can satisfy the requirement of undergoing 20 times the designed wind load if all the components are ideally connected, so the value of the ultimate strength would be much smaller if real bolt connections are used.



**Figure 23. Global deformation shape of the portal frame under designed wind load**

The deformation shape of the portal frame model with 40×40mm meshes under 0.06 MPa wind load is magnified with a 5% scaling factor relative to the whole dimension of the portal frame, as the deflection may be very tiny and hard to recognize compared to the large dimension of the whole structure. The reason for choosing the coarse meshed model for the deformation shape demonstration is that the changes in the configuration shape of the finer meshed ones can hardly be represented in a small size figure, as the dense grid lines hide the contour colors. As is indicated in the Figure 23, a maximum horizontal deflection of 8.82 mm was found when the wind load reached the required value of 0.06 Mpa. The maximum relative horizontal displacement occurred in the flange of the left loaded eave bracket. Flexural-torsional buckling was found all over the members with no local damage. The flange of the left eave bracket was compressed inwardly due to the horizontal loading, and the right eave bracket was propped up outwardly due to the flexural-torsional buckling deformation of

the adjacent members. One possible reason may be the thin-walled structure of CFS members with wide webs and relatively narrow flanges, which makes the members easy to turn around under the eccentric loading with their ends being fully restrained. Meanwhile, only the outermost flanges were restrained to avoid large out-of-plate deflection according to the real construction condition, and this did not necessarily prevent the inner flanges from bending inwards or outwards, which contributed to the global flexural-torsional buckling in some way. One possible solution to this problem is to install bracing at the eave bracket corners to decrease the out-of-plate bending of the flange on the inner edge.

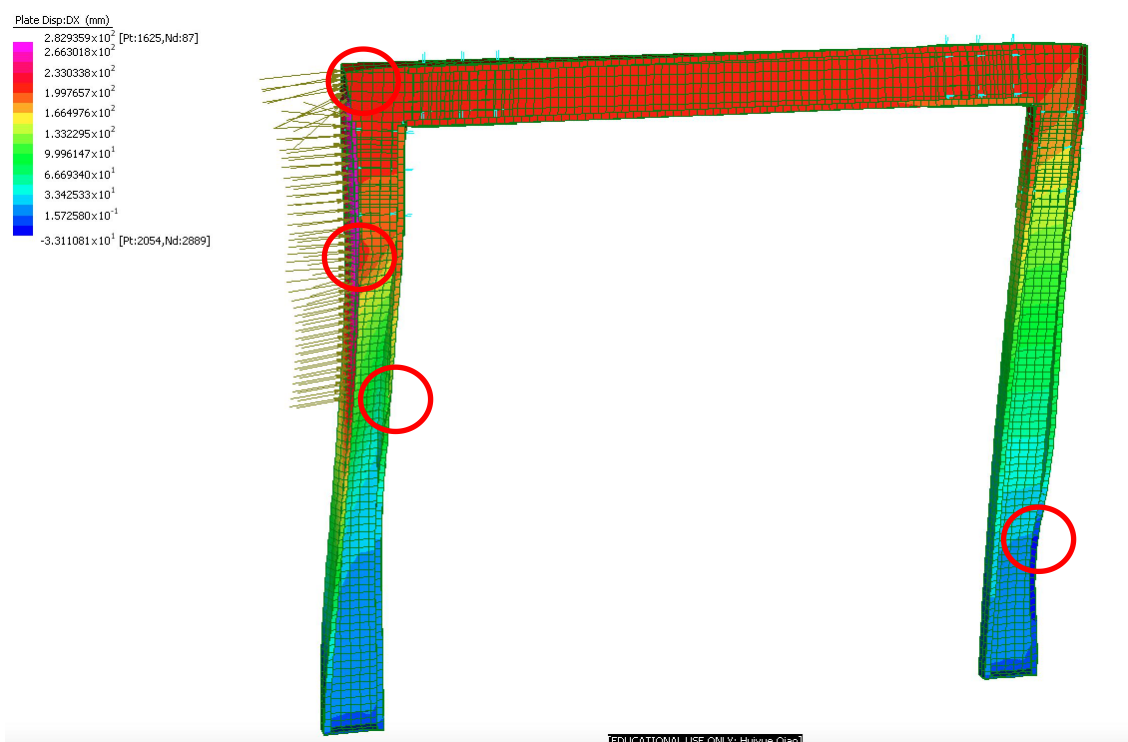


**Figure 24. Deformation shape of the portal frame model at the ultimate load.**

At the ultimate load of 1.2MPa, the local flange distortional buckling and local web buckling were found on the columns of the ideally connected CFS portal frame model, as marked in Figure 24. The reason for the local flange and web deformation may be the large external loading plus large flexural-distortional buckling of members, and local buckling has a high possibility of occurring near the points of contraflexure of the heavily twisted members.

### 4.3 Estimation of the true frame strengths considering bolt capacity

In real construction, the capacity of each bolt can significantly influence the strength behaviour of the CFS portal frame. This research used rigid link elements to replace the modelling of real bolts. The shear forces which are estimated to be supported by bolts can be captured by checking the forces of the pair of nodes linked by rigid link elements. The corresponding two nodes are supposed to have the same value of internal force but with opposite directions. The maximum shear force allowed for each bolt is approximately 3 kN, as found in prevalent engineering practice.

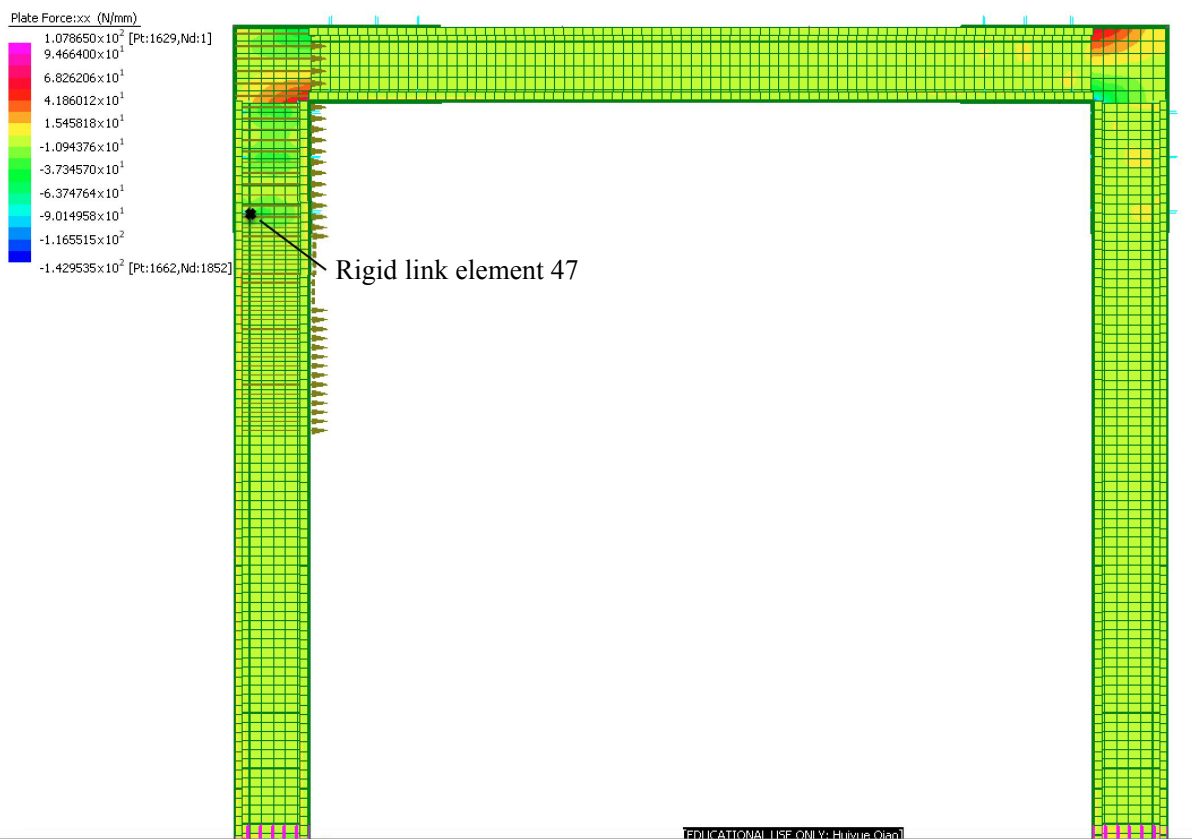
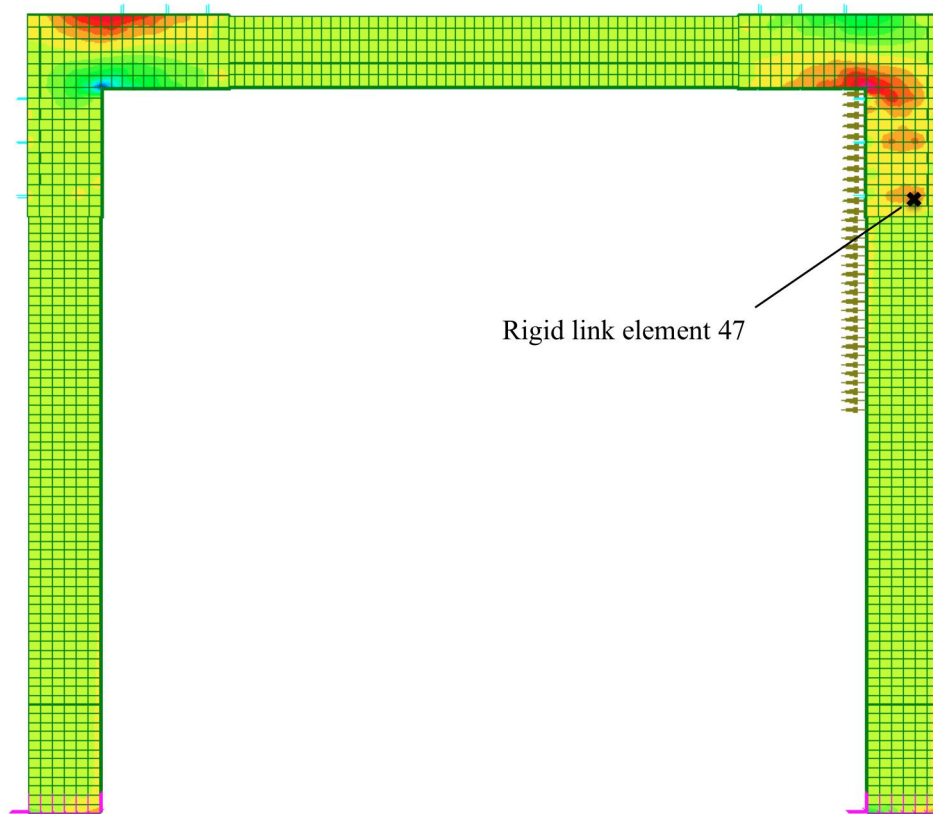


Figure 25. Plate force contour plot front view.

In the mesh, each node is at the intersection of four adjacent plate elements. The node force can be derived from the plate force result list by adding the separate forces of that node over the 4 plate elements together. After several trials, the pair of nodes connected by rigid link element 47 was found to have the largest internal node forces among all the pairs of nodes connected by rigid link elements. Rigid link 47 is located in the region of high plate forces in

the whole structure, where the plate force contour colour is red. Its location is marked in the plate force contour plot in Figure 25 and Figure 26.



**Figure 26. Plate force contour plot back view**

It was found that at the lateral load of 0.039 MPa, the pair of nodes linked by number 47 rigid link elements both have the same value of internal force of 3 KN with opposite directions, which reaches the maximum shear force value for the bolt supposed to be located there. The separate forces of each node from its adjacent 4 plates are shown in Table 2.

However, this doesn't mean that the whole structure will fail immediately when the applied lateral load reaches 0.039 MPa. Under the hypothesis that all the bolts are installed at the same location of the rigid link elements, the bolt installed at the location of rigid link element 47 will have the largest capacity reduction first since it needs to sustain relatively higher plate forces than other bolts. Bolts located at different places in the model will lose their best function gradually after 0.039 MPa.

**Table 2. Internal forces of nodes linked by rigid link element 47 at 0.039 MPa applied force.**

Node 1452		Node 1614	
Plate number	Separate node force FX (KN)	Plate number	Separate node force FX (KN)
522	1.03	43	-0.71
964	0.93	1443	-1.04
1163	0.79	1444	-0.4
1364	0.25	1565	-0.85
Total FX(KN)	3		-3

In the meantime, the distribution of the node force magnitudes at the potential bolt locations is uneven. However, in general, bolts installed on the left part of the CFS portal frame tend to sustain larger shear forces than those on the right part, which can be inferred from Figures 25 and 26. The rigid link nodes located at the stacked web of members were found to have higher node forces than those at the stacked flanges.

The CFS portal frame was estimated to sustain at least 1.5 times the designed 0.06MPa wind load considering the strength of bolts. Figure 27 below shows the distribution of node force values at the location of potential web bolts in the left part of the frame. At that time, the applied wind load reached 0.09 MPa, which is 1.5 times the designed wind load. The node force values shown in Figure 27 are from the column and the beam plates, which indicate the shear force of the bolts from the upper plate along the X axis. Shear forces with opposite directions can be found at the same locations on the eave bracket plate, which is the lower plate for bolts.

As is indicated from Figure 27, when the applied distributed wind load reached 1.5 times the designed wind load, a maximum of 6.95 KN of node force was found at the location of the real bolt on the column web, and a negative value of -6.95 KN of node force also existed on the web of the eave bracket on the back of the column web. This means that the bolt installed at that location needs to sustain a pair of 6.95 KN shear forces in opposite directions, which exceeds the estimated capacity for a single bolt of a maximum of 3KN shear forces. In this way, tearing of steel plates may occur at the connection part in the CFS portal frame due to the extra loading around the location of bolts, but this would not necessarily lead to the direct failure of the model.

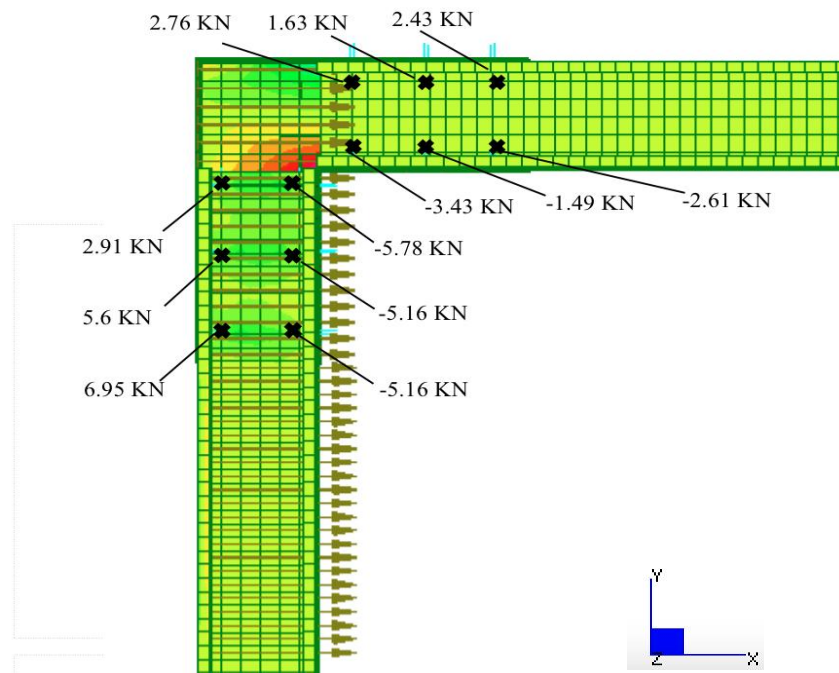


**Figure 27. Estimated bolt forces on the left top corner of portal frame**

## 5 CONCLUSION

This research detected the lateral resistance of a non-apex portal frame consisting of CFS members with single-C shaped profiles. To verify if this CFS portal frame can substitute the use of the hot-rolled PFS portal frame in residential construction, a full-scale finite element model using Quad4 elements in Strand7 was built to explore its capacity to work as a load-carrying structure, with rigid link elements working as idealised connections. The total span of the finite element portal frame model is 3.2 m and the height is 2.8 m.

The finite element model with the coarse mesh was used to validate the accuracy of the modelling method under static linear analysis, and the function of the rigid link elements was also verified using plate elements. Then the Advanced Analysis method excluding the influence of imperfections was applied, taking advantage of the Strand7 static nonlinear solver. The load increments were controlled by gradually increasing load factors under the Newton-Raphson technique. After the convergence study of load-displacement results derived from models with different mesh sizes, it was shown that a portal frame structure made of ideally connected C-shaped CFS members has a yield strength of 1.15 MPa and can

finally sustain an ultimate load of 1.2 MPa. At the design wind load of 0.06 MPa, the ideally connected structure is still under the elastic deformation phase with 8.82 mm of horizontal displacement. The effects of bolts were estimated from the node forces at the location of real bolts where upper and lower plates stacked together. Each bolt is supposed to have an ultimate capacity of 3 KN under shear forces from construction experience. When the applied load reaches 0.039 MPa, the bolt installed at the location of rigid link 47 would attain its shear force capacity, with other bolts losing strength gradually. At the load of 1.5 times the wind load, the largest node forces were found at the location of link 47 with 6.57KN on upper and lower plates in opposite directions, and tearing may occur between the CFS plates and deformed bolts.

So, it can be concluded that the capacity of the CFS portal frame model using rigid link elements is much higher than the actual capacity of the CFS portal frame using bolts. In reality, possible tearing may occur between bolts and CFS plates on the portal frame due to the early deformation of bolts. During the deformation process, flexural-torsional bulking appeared in the whole structure model with some local damage on the member webs and flanges near the ultimate load.

Lessons were also found during the research process. The CFS model was idealised with many assumptions, like using rigid link elements to replace the bolts, using base plates with transition restrained nodes to simulate the function of support, and so on, which cannot precisely simulate the real condition. As a result of this, the inaccuracy of simulation results can be normal. The capacity of the CFS portal frame model may be bigger than expected if using rigid link elements or smaller than expected if considering the effects of bolts. Meanwhile, to simulate the behaviour of a physical structure, the modelling process needs to be validated carefully to check the accuracy of the model. Moreover, it was found from the results that the bolt connections can affect the strength of the structure largely, even though the CFS frame is proved to be very tough under lateral loads if all the different components are composed ideally, so the estimation of the bolt strength is quite necessary after the structure behaviour is simulated using rigid link elements.

The CFS portal frame using single-C opening cross sections has proved to be tough enough under lateral loading if all the members are composed perfectly. Tearing between bolts and

CFS plates may happen under the designed lateral load, but the structure can still be used in the structural system in residential buildings, hopefully. By incorporating cold-formed portal frames into on-site residential construction to replace costly hot-rolled portal frames, consumption on delivery and assembly costs can be significantly reduced, resulting in cost-effective construction. However, future research on the vertical load resistant performance and combined load resistance of the CFS portal frame is needed before the frame is put into industry, and specific studies of the effect of bolts using experimental methods or modelling simulation are still required.

## 6 REFERENCES

- ÁDÁNY, S., & SCHAFFER, B. (2004). Buckling Mode Classification of Members with Open Thin-walled Cross-sections. *Fourth International Conference on Coupled Instabilities in Metal Structures*, 27–29.
- Baigent, A. H., & Hancock, G. (1981). The stiffness and strength of portal frames composed of cold-formed members. *Australia: Civil Engineering Transaction, the Institution of Engineers, CE 24(3)*, 278–283.
- Blum, H. B., & Rasmussen, K. J. R. (2019). Experimental investigation of long-span CFS double channel portal frames. *Journal of Constructional Steel Research*, 155, 316–330. <https://doi.org/10.1016/j.jcsr.2018.11.020>
- Baran, E., & Alica, C. (2002). Behavior of cold-formed steel wall panels under monotonic horizontal loading. *Journal of Constructional Steel Research*, 79, 1-8. <https://doi.org/10.1016/j.jcsr.2012.07.020>.
- Camotim, D., Silvestre, N., & Dinis, P. B. (2005). Numerical Analysis of CFS Members. *Steel Structures*, 5, 63–78.
- Chen & Kim, S.-E. (1997). *LRFD steel design using advanced analysis*. Crc Press.
- Chen, H., Schafer, B., & LaBoube, R. (2007). Direct Strength Method for CFS. *STRUCTURE*.
- Cheng, Y. (2005). *Distortional buckling of CFS members in bending* [PhD Thesis]. <http://jhir.library.jhu.edu/handle/1774.2/40577>
- Chu, X., Kettle, R., & Li, L. (2004). Lateral-torsion buckling analysis of partial-laterally restrained thin-walled channel-section beams. *Journal of Constructional Steel Research*, 60(8), 1159–1175. <https://doi.org/10.1016/j.jcsr.2003.11.001>
- Dabaon, M., Ellobody, E., & Ramzy, K. (2015). Nonlinear behaviour of built-up CFS section battened columns. *Journal of Constructional Steel Research*, 110, 16–28. <https://doi.org/10.1016/j.jcsr.2015.03.007>
- Davies, J. M., Engel, P., Liu, T. T. C., & Morris, L. J. (1990). Realistic modelling of steel portal frame behaviour. *Structural Engineer*, 68, 1–6.
- Dundu, M. (2011). Design approach of CFS portal frames. *International Journal of Steel Structures*, 11(3), 259–273. <https://doi.org/10.1007/s13296-011-3002-2>
- Gardner, L., & Yun, X. (2018). Description of stress-strain curves for CFSs. *Construction and Building Materials*, 189, 527–538. <https://doi.org/10.1016/j.conbuildmat.2018.08.195>

- Gotluru, B. P., Schafer, B. W., & Peköz, T. (2000). Torsion in thin-walled CFS beams. *Thin-Walled Structures*, 37(2), 127–145. [https://doi.org/10.1016/s0263-8231\(00\)00011-2](https://doi.org/10.1016/s0263-8231(00)00011-2)
- Grubb, P. J., Gorgolewski, M. T., & Lawson, R. M. (2001). Building Design using in Cold Formed Steel Section: Light Steel Framing in Residential Construction. *The Steel Construction Institute*.  
[https://www.steelconstruction.info/images/3/38/SCI\\_P301.pdf](https://www.steelconstruction.info/images/3/38/SCI_P301.pdf)
- Hancock, G. J., Murray, T., & Ellifrit, D. S. (2001). *CFS Structures to the AISI Specification*. Taylor & Francis.
- Hancock, G. J. (2003). Cold-formed steel structures. *Journal of Constructional Steel Research*, 59 (4), 473-487. [https://doi.org/10.1016/S0143-974X\(02\)00103-7](https://doi.org/10.1016/S0143-974X(02)00103-7).
- Harini, B., Lingeshwaran, N., Perumal, K., & Aravinthan, K. (2020). *Stainable design of cold formed steel*. *Materials Today: Proceedings*, 33(1), 881-885.  
<https://doi.org/10.1016/j.matpr.2020.06.406>
- Kim, S.-E., & Chen, W.-F. (1999). Design guide for steel frames using advanced analysis program. *Engineering Structures*, 21(4), 352–364. [https://doi.org/10.1016/s0141-0296\(97\)00209-5](https://doi.org/10.1016/s0141-0296(97)00209-5)
- Lue, D. M., Chung, P.-T., Liu, J.-L., & Pan, C.-L. (2009). The compressive strength of slender C-shaped CFS members with web openings. *International Journal of Steel Structures*, 9(3), 231–240. <https://doi.org/10.1007/bf03249497>
- Mohite, P. M., & Karoo, A. C. (2015). Buckling Analysis of Cold Formed Steel for Beams. *International Journal of Scientific and Research Publications*, 5(5), 543–549.  
<https://doi.org/10.1.1.735.3953>
- Mojtabaei, S. M., Kabir, M. Z., Hajirasouliha, I., & Kargar, M. (2018). Analytical and experimental study on the seismic performance of CFS frames. *Journal of Constructional Steel Research*, 143, 18–31.  
<https://doi.org/10.1016/j.jcsr.2017.12.013>
- Naderian, H. R., & Ronagh, H. R. (2015). Buckling analysis of thin-walled CFS structural members using complex finite strip method. *Thin-Walled Structures*, 90, 74–83.  
<https://doi.org/10.1016/j.tws.2015.01.008>
- Neal, B. G. (1977). *The plastic methods of structural analysis*. Chapman And Hall.
- Phan, T., Lim, J., Selowara Joo, M., & Lau, H.-H. (2017). Design Optimization of Long-Span CFS Portal Frames Accounting for Effect of Knee Brace Joint Configuration. *Technologies*, 5(4), 81. <https://doi.org/10.3390/technologies5040081>

- Qing Quan Liang. (2015). *Analysis and design of steel and composite structures*. Crc Press/Taylor & Francis Group.
- Ramberg, W., & Osgood, W. R. (1943). *Description of stress-strain curves by three parameters*. National Advisory Committee For Aeronautics.  
<https://ntrs.nasa.gov/api/citations/19930081614/downloads/19930081614.pdf>
- Rinchen. (2018). *Long-span CFS single C-section portal frames*. Ses.library.usyd.edu.au.  
<http://hdl.handle.net/2123/18882>
- Rinchen, R., & Rasmussen, K. J. R. (2020). Experiments on Long-Span CFS Single C-Section Portal Frames. *Journal of Structural Engineering*, 146(1), 04019187.  
[https://doi.org/10.1061/\(asce\)st.1943-541x.0002487](https://doi.org/10.1061/(asce)st.1943-541x.0002487)
- Rinchen, & Rasmussen, K. J. R. (2019). Numerical modelling of CFS single C-section portal frames. *Journal of Constructional Steel Research*, 158, 143–155.  
<https://doi.org/10.1016/j.jcsr.2019.03.024>
- Rinchen, Rasmussen, K. J. R., & Zhang, H. (2019). Design of CFS single C-section portal frames. *Journal of Constructional Steel Research*, 162, 105722.  
<https://doi.org/10.1016/j.jcsr.2019.105722>
- Sena Cardoso, F., & Rasmussen, K. J. R. (2016). Finite element (FE) modelling of storage rack frames. *Journal of Constructional Steel Research*, 126, 1–14.  
<https://doi.org/10.1016/j.jcsr.2016.06.015>
- Sena Cardoso, F., Zhang, H., Rasmussen, K. J. R., & Yan, S. (2019). Reliability calibrations for the design of CFS portal frames by advanced analysis. *Engineering Structures*, 182, 164–171. <https://doi.org/10.1016/j.engstruct.2018.12.054>
- Strand7 Pty Ltd. (n.d.). *Strand7 (student version)* . [Computer Software].  
<https://www.strand7.com/student/>
- Tan, S. H. (2001). Channel frames with semi-rigid joints. *Computers & Structures*, 79(7), 715–725. [https://doi.org/10.1016/s0045-7949\(00\)00173-5](https://doi.org/10.1016/s0045-7949(00)00173-5)
- Torkamani, M. A. M., & Sonmez, M. (2008). Solution Techniques for Nonlinear Equilibrium Equations. *Structures Congress 2008*, 315(978-0-7844-1000-4).  
[https://doi.org/10.1061/41000\(315\)35](https://doi.org/10.1061/41000(315)35)
- Trahair, N. S. (2012). Trends in the analysis and design of steel framed structures. In <http://sydney.edu.au/civil>.  
<https://ses.library.usyd.edu.au/bitstream/handle/2123/24051/r926.pdf?sequence=1&isAllowed=y>

Trahair, N. S., Bradford, M. A., Nethercot, D. A., & Gardner, L. (1977). *The Behaviour and design of steel structures to EC3 (4th ed.)*. CRC Press.

Ye, J., Hajirasouliha, I., Becque, J., & Pilakoutas, K. (2016). Development of more efficient CFS channel sections in bending. *Thin-Walled Structures*, *101*, 1–13. <https://doi.org/10.1016/j.tws.2015.12.021>

Yu, W. W., LaBoube, R. A., & Chen, H. (2020). Cold-Formed Steel Design (5th Edition) - 1.1 General Remarks, 1.2.1 Individual Structural Framing Members. John Wiley & Sons. <https://app.knovel.com/hotlink/pdf/id:kt012EMQX3/cold-formed-steel-design/panels-and-decks>

Zhang, X., Rasmussen, K. J. R., & Zhang, H. (2015). Structural modeling of CFS portal frames. *Structures*, *4*, 58–68. <https://doi.org/10.1016/j.istruc.2015.10.010>

## 7 APPENDIX

**Table A.1 Load and displacement data for portal frame models of different mesh sizes.**

Load (MPa)	Displacement (mm)		
	40*40mm	20*20mm	10*10mm
0.01	0.66	0.68	0.68
0.50	43.12	43.20	43.28
0.90	74.72	72.62	72.96
0.95	77.52	77.38	77.60
0.96	118.89	77.99	78.25
0.965	119.79	78.30	78.57
0.97	120.80	78.59	78.89
0.98	123.72	79.16	79.51
0.99	128.05	79.73	80.11
1.00	130.21	80.26	80.70
1.05	146.27	82.00	82.81
1.10	168.71	84.10	85.03
1.15	189.95	187.48	95.44
1.20	225.98	285.93	235.52

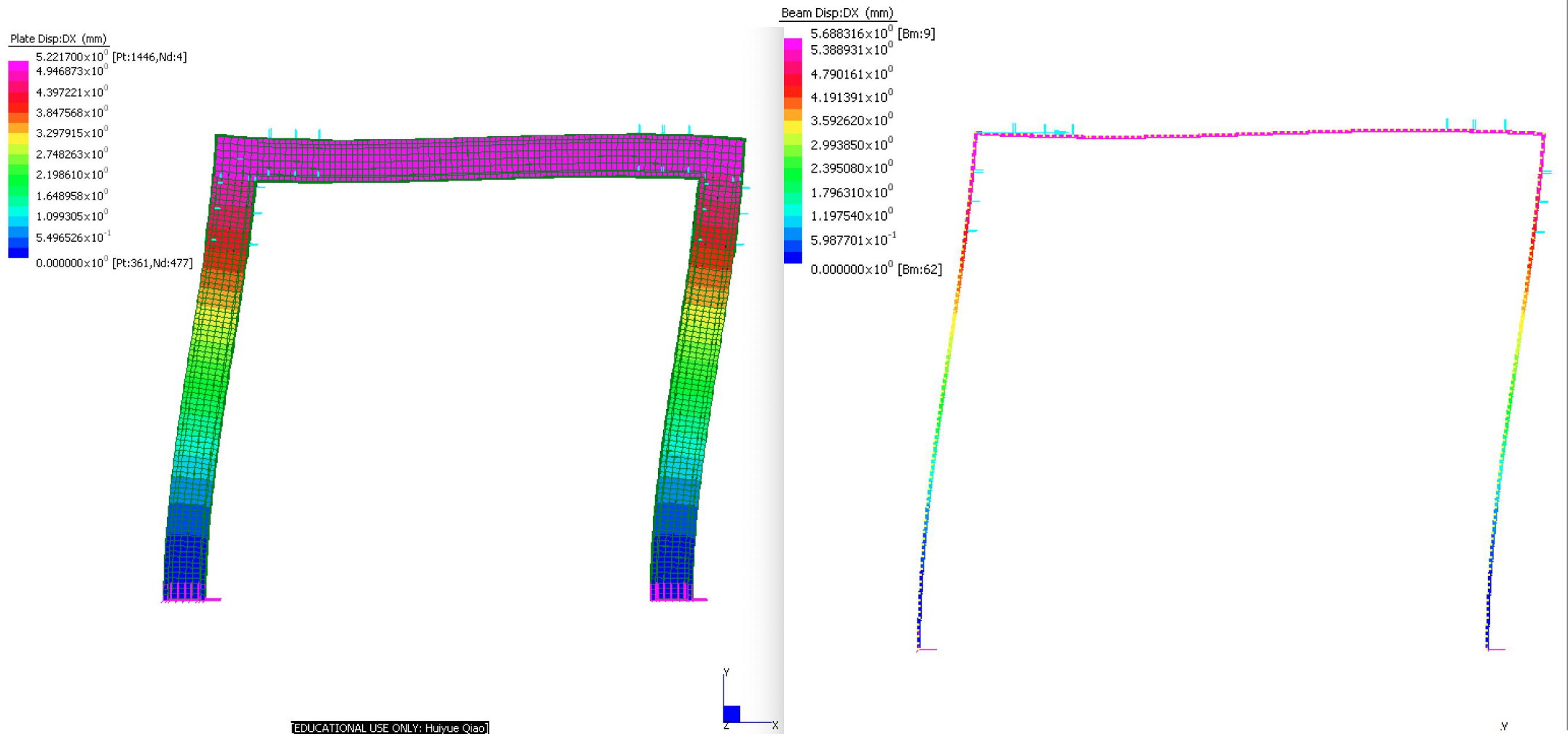


**Figure A.1 Displacement value and deformation shape comparison between the plate element model and the beam element model**

**Table A.2 Node reaction data of rigid link element validation test.**

Node	1	2	3	4	5	6	7	8	9	10	11	12	13	14	15	16	17	18
FX (N)	0	0	0	0	0	0	0	0	0	0	0	-2	0	-2	0	0	-2	-2